RSC Sustainability

ROYAL SOCIETY OF CHEMISTRY

CRITICAL REVIEW

View Article Online
View Journal | View Issue

Open Access Article. Published on 12 February 2026. Downloaded on 3/23/2026 6:55:17 AM.
This article is licensed under a Creative Commons Attribution 3.0 Unported Licence.

Check for updates

Cite this: *RSC Sustainability*, 2026, **4**, 1252

Polyaniline-based ternary composites for the photocatalytic degradation of organic pollutants in wastewater: multifunctional properties, synthetic routes, and mechanistic insights

Jyoti Kumari,[a] Adarsh Singh,[a] Akash Rawat,[b] Suneel Kumar Srivastava[c] and Ashok Kumar Gupta *[a]

Received 7th July 2025
Accepted 9th February 2026

DOI: 10.1039/d5su00570a

rsc.li/rscsus

The widespread applications of pharmaceuticals, pesticides, dyes, and industrial chemicals have caused extensive contamination of water resources globally. Conventional wastewater treatment processes have been inefficient for the elimination of these contaminants, resulting in their sustained accumulation. Among advanced oxidation processes (AOPs), photocatalysis has garnered notable attention as an effective method for the degradation of organic pollutants owing to its ability to achieve complete mineralization. However, the degradation performance of conventional single and binary composites remains constricted by rapid electron–hole recombination, limited light absorption ability, and material instability. Recent research has been focused on the development of ternary composite systems incorporating conducting polymers, which synergistically utilize the unique advantages of organic and inorganic components to enhance the photocatalytic efficiency. Particularly, polyaniline (PANI) has emerged as a promising conducting polymer owing to its simple synthesis, tunability, electrical conductivity, environmental stability, and efficient electron transport properties. This review provides a comprehensive analysis of the synthesis and properties of PANI and its application in ternary composites. The PANI-based ternary composites have been further evaluated for their synthetic routes, photocatalytic degradation mechanism, applicability, stability, and reusability, confirming their efficiency as photocatalysts. Additionally, their key challenges and limitations are critically evaluated, and future research directions are proposed to advance PANI-based ternary composites for sustainable wastewater treatment.

Sustainability spotlight

Polyaniline (PANI)-based ternary photocatalysts signify a promising way for sustainable wastewater treatment owing to their intrinsic property to cater visible-light responsiveness, redox potential, and interfacial structures, enabling pollutant degradation under low-energy irradiation. The integration of conducting polymers with other semiconductor components offers a way to lessen the compliance over UV-driven sources and enhance the energy efficiency. PANI-based composites offer significant flexibility for greener synthesis strategies. Moreover, these composites are stable and can be reused multiple times for wastewater treatment. By integrating proper reactor design, toxicity assessment, reproducibility and performance evaluation, PANI-based ternary composites can be scaled up for wastewater treatment, helping to achieve Sustainable Development Goal (SDG) 6: clean water and sanitation.

1. Introduction

In recent years, the widespread occurrence of organic pollutants in wastewater has become a global issue, posing significant risks to both environmental safety and human health.[1–4] These substances are also referred to by different names, such as emerging contaminants (ECs),[5–8] emerging pollutants (EPs),[9] contaminants of emerging concerns (CECs),[8,10] trace organic compounds (TrOCs), and micropollutants (MPs).[11] These contaminants, due to their extensive use, are often found in environmental matrices and include a wide range of highly polar, acidic, and alkaline substances like pharmaceuticals and personal care products (PPCPs),[12–14] dyes,[15] pesticides,[16] surfactants, phenolic compounds,[17–19] perfluorinated substances,[20] and polycyclic aromatic hydrocarbons (PAHs).[8,21–24] Moreover, some ECs are classified as endocrine-disrupting chemicals

[a]*Environmental Engineering Division, Department of Civil Engineering, Indian Institute of Technology Kharagpur, Kharagpur 721302, India. E-mail: agupta@civil.iitkgp.ac.in*

[b]*School of Environmental Science and Engineering, Indian Institute of Technology Kharagpur, Kharagpur 721302, India*

[c]*Department of Chemistry, Indian Institute of Technology Kharagpur, Kharagpur 721302, India*

© 2026 The Author(s). Published by the Royal Society of Chemistry

Open Access Article. Published on 12 February 2026. Downloaded on 3/23/2026 6:55:17 AM. This article is licensed under a Creative Commons Attribution 3.0 Unported Licence.

(EDCs) due to their hydrophobic nature, which leads to their accumulation in the lipid-rich tissues of living organisms. These chemicals can disrupt endocrine systems and also contribute to the development of antimicrobial resistance. EDCs have been linked to health problems like endometriosis and cancers.[8,23,25–28] Therefore, it is very crucial to treat these compounds in wastewater to ensure the safety of human life and the environment.

Conventional methods like membrane filtration, ultrafiltration, activated carbon-based adsorption, Fenton oxidation, advanced oxidation processes (AOPs), electrochemical oxidation, and ozonation have been reported to effectively remove organic pollutants from water and wastewater.[10,29–33] However, the choice of the aforementioned conventional methods is guided by several limitations, *e.g.*, membrane filtration, ozonation, and activated carbon-based adsorption being costly, energy-intensive, and less effective.[34] In this perspective, AOPs are considered one of the most promising techniques for the removal of ECs from aqueous matrices.[35–38] Particularly, photocatalysis has emerged as a prominent treatment solution for remediating various kinds of ECs from water and wastewater.[39,40] The photocatalytic process is initiated by exposing the photocatalyst to a light source such as ultraviolet (UV) light, visible light, natural sunlight, or simulated sunlight produced through an artificial source. When the energy of the incoming photon is greater than the band gap (E_g) of the photocatalyst, the electron (e^-) in the valence band (VB) gets excited and jumps to the conduction band (CB), thereby creating a hole (h^+) in the VB. These e^-/h^+ pairs are responsible for the formation of active radicals, referred to as reactive oxygen species (ROS), which ultimately mineralize the contaminants to form H_2O and CO_2.[41,42] However, pristine photocatalysts face certain limitations: (i) recombination of photogenerated e^-/h^+ pairs and (ii) limited utilization of incident light and photo-corrosion.[43] Reportedly, the aforementioned limitations can be overcome by elemental doping, defect creation, and combination with other semiconducting materials through heterojunction formation.[44–49] In recent years, research has shifted to synthesizing ternary composite photocatalysts due to their inherent advantages and superior photocatalytic efficiency compared to other improvement techniques.[50] The composite material exhibits enhanced light absorption capacity, improved charge separation, synergistic effect of individual components, enhanced stability, and reusability.[51,52]

In recent years, research has increasingly focused on employing conducting polymers to enhance the photocatalytic efficiency. These are special types of polymers that can conduct electricity like semiconductors or metals and exhibit combined electrical and optical properties of both organic materials and inorganic substances.[53–55] This is due to the presence of alternate conjugated carbon chains comprising single and double bonds along the chain, which accounts for its highly delocalized e^- within the molecule.[53,54,56] These delocalized e^- are free to move across the chain, making the structure electron-rich and highly polarized.[53] The extended π–e^- system in conducting polymers improves the stability and charge carrier mobility.[57] Conducting polymers may exhibit either an amorphous or a crystalline nature. The presence of π-bonds in their molecular structure gives them exceptional capabilities for charge transport and light harvesting capability.[58] The conducting polymers comprise PANI,[59] polypyrrole,[60] poly(3,4-ethylenedioxythiophene) (PEDOT),[61] polythiophene,[62] polyacetylene,[63] polyfuran,[64] and polyparaphenylene.[65] Among others, polyaniline (PANI) has attracted significant attention in the field of photocatalysis owing to its distinct advantages such as ease of preparation, remarkable stability, enhanced light absorption, and reduced charge carrier recombination.[66–68] Furthermore, PANI exhibits a unique conjugation phenomenon, high absorption coefficient, protonation reversibility, superior redox properties, resistance to photobleaching, ease of structural modification and photocatalytic sensitivity. These multifaceted properties, along with cleaner and sustainable processes, collectively compel future research and studies.[69]

To date, several review articles have investigated the use of PANI-based binary composites for photocatalytic degradation.[70–72] Although binary systems have shown considerable potential, they often suffer from inherent limitations such as lower redox activity, reduced visible-light response, and inefficient charge separation,[50] which eventually affect the photocatalytic performance. Consequently, recent research has gradually shifted toward ternary nanocomposites, which integrate multiple functional components to overcome the limitations associated with binary heterojunctions. For instance, Prasad *et al.*[73] reported g-C_3N_4-based ternary nanocomposites, highlighting their enhanced visible-light utilization and improved charge carrier separation. With the same context, G. G. *et al.*[74] examined graphene-based ternary systems for the removal of both cationic and anionic pollutants, emphasizing graphene's role in facilitating electron transport. Likewise, Roopan and Khan[50] presented a comprehensive review of MoS_2-based ternary composites for wastewater treatment *via* photocatalytic degradation. In addition, Kanakaraju and Chandrasekaran[75] highlighted TiO_2/ZnS-based ternary nanocomposites, demonstrating their versatility across various applications, including photocatalysis.

Over the past decade, PANI-based ternary composites have been increasingly explored for photocatalytic applications, particularly in wastewater treatment. However, to the best of our knowledge, a state-of-the-art critical review dedicated specifically to PANI-based ternary nanocomposites has not yet been reported. In this context, the present review systematically examines PANI-based ternary composites, with a particular focus on heterojunction design, charge transfer mechanisms, and photocatalytic performance in the removal of organic pollutants. Additionally, issues related to stability, sustainability, and practical applicability are thoroughly discussed. By consolidating dispersed studies into a unified framework, this review highlights how ternary architectures effectively overcome the limitations of individual and binary systems.

In this regard, this review first details the aspects of PANI chemistry, including its properties and synthesis routes in the context of photocatalysis function. Further, it examines its integration with inorganic, carbonaceous, and metal oxides for the construction of ternary structures, highlighting the design

Open Access Article. Published on 12 February 2026. Downloaded on 3/23/2026 6:55:17 AM.
This article is licensed under a Creative Commons Attribution 3.0 Unported Licence.

principles, charge transfer, and pollutant-specific reactivity. The review evaluates the photocatalytic performances, degradation pathways, stability, and reusability for developing sustainable approaches. Key challenges and literature gaps have been identified, and future directions have been proposed for scalable wastewater treatment technologies.

2. Structure and properties of PANI

PANI has the basic structural formula of $[(-B-NH-B-NH-)_y(-B-N{=}Q{=}N-)_{1-y}]_x$, where B and Q represent the C_6H_4 rings in the benzenoid and quinonoid forms, respectively, connected by N atoms in the backbone.[76,77] PANI exists in various oxidation states, pernigraniline is fully oxidized (PNA, where $y = 0$), leucoemeraldine is fully reduced (LM, $y = 1$), emeraldine is half oxidized (EM, $y = 0.5$) and the last form is nigraniline which is 75% oxidized (NA, $y = 0.75$),[76–79] as displayed in Fig. 1. Among all oxidation states of PANI, EM base is most widely used for application in photocatalysis due to its ability to convert itself as conductive EM salt on doping with protonic acid. This form is very dissimilar from other existing states of PANI, *i.e.*, the leucoemeraldine state, which is a reduced state with only benzenoid rings, and the pernigraniline state, which is entirely oxidized and has a quinoid ring as a repeating unit.[53,80–83] Various properties of PANI are discussed below.

2.1. Magnetic properties

PANI has attracted considerable attention due to its magnetic behaviour, as it exhibits high spin density due to the doping of protonic acid (such as HCl, H_2SO_4, or organic acids) during the oxidation process.[80,84–88] Moreover, the protonic acid doping introduces radical cations (polarons) into the PANI backbone, resulting in a substantial increase in paramagnetic centers.[89] The presence of these unpaired spins is responsible for the observed paramagnetic behaviour in doped PANI.[90]

2.2. Redox properties

PANI exhibits exceptional redox properties, as demonstrated by its ability to reversibly transition between various oxidation states through the acceptance or donation of electrons, which contributes to its diverse electrochemical applications.[80] Reportedly, PANI maintains strong electrochemical activity and reduction potential to account for its applications in energy storage devices.[91] It is well established that the fast oxidation and reduction processes that occur within the polymer structure in PANI increase the performance of energy storage devices, as indicated by its high capacitive response and superior energy storage ability compared to the double-layered capacitors.[87]

2.3. Electrical properties

The electrical properties of PANI are due to its ability to conduct electricity in the EM salt form.[87] When an acid is introduced to the half-oxidized state of PANI, *i.e.*, EM base form, it protonates nitrogen in the imine group, which converts it into an EM salt leading to conversion in the conductive form.[92,93] The conductivity of PANI is closely linked to the formation of charge carriers during the doping process and the ability to transfer electrons.[94,95] The dopant (such as HCl and H_2SO_4) remains chemically unbound with the PANI main structure and does not change its chemical property, though it provides polymer chain vicinity to dopants facilitating charge carrier transport.[53,96] The presence of protonic acid as a dopant in PANI during the oxidation process enhances its conductivity owing to the enhanced charge carrier mobility along the polymer chains.[97]

2.4. Optical properties

The optical properties of PANI are used in determining its oxidation state and protonation process.[87] According to Huang and MacDiarmid, a blue shift is observed from 3.94 to 4.17 eV

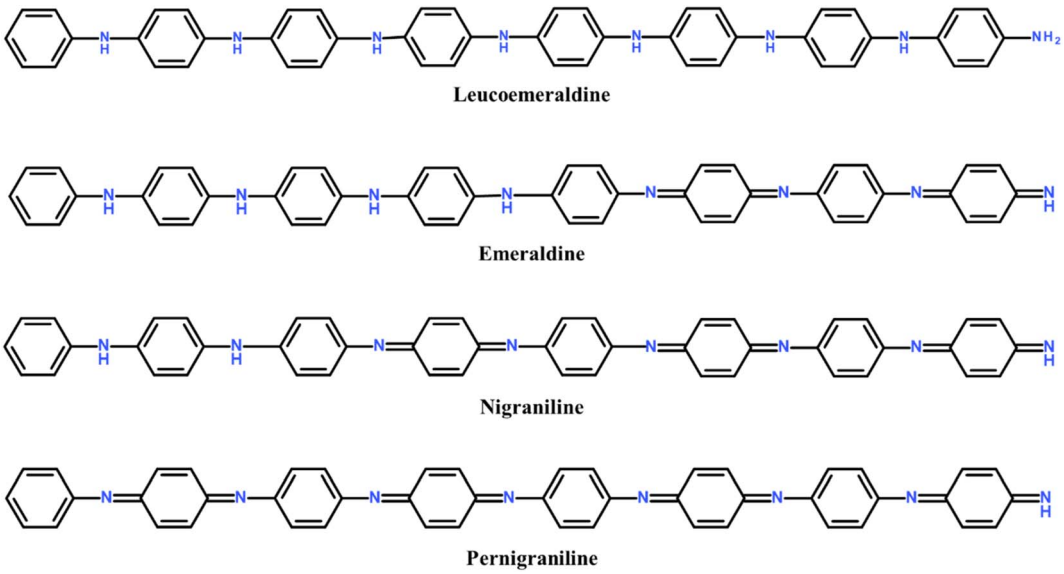

Fig. 1 Structural representation of the various forms of PANI.

 © 2026 The Author(s). Published by the Royal Society of Chemistry

Open Access Article. Published on 12 February 2026. Downloaded on 3/23/2026 6:55:17 AM. This article is licensed under a Creative Commons Attribution 3.0 Unported Licence.

during the conversion of leucoemeraldine from its base to salt form and ascribed to the e^- excitation between the highest occupied molecular orbital (HOMO) and the lowest unoccupied molecular orbital (LUMO) levels with the absorption peak at 2.1 eV.[98] PANI in the oxidized state shows an absorption spectrum consisting of two peaks in the UV-vis range 3.8 eV (π–π transition) and 2.75 eV and one peak in the near-infrared (NIR) range 1.5 eV.[99] The EM salt shows three characteristic absorption bands in its structure around 360 nm (π–π transition), 780 nm (π to polaron band), and 440 nm (polaron to π).[100–102]

2.5. Anti-corrosive property

Corrosion is the chemical reaction that affects metal due to the environmental factors present near its surroundings.[86,103] In this regard, PANI is used as an anti-corrosive material due to its ennobling effect on the metal surface and self-healing mechanism.[104,105] Studies show that PANI with a sulfate dopant layer is more effective in reducing corrosion than PANI with a phosphate layer, as the phosphate counterion hinders the autocatalytic oxidation of aniline, leading to reduced oxide formation on the electrode surface.[87,106] Materials such as nickel, and tungsten with PANI are being used for protecting steel and iron from corrosion employing the self-healing property of PANI, protecting pinholes by releasing dopant anions, leading to the formation of secondary physical barrier.[107–109]

3. Synthesis of PANI

PANI is regarded as a prominent electrically conducting polymer due to its ability to transition easily between base and salt forms. This transformation can be achieved simply by adding a base and an acid.[87] PANI has unique properties such as excellent electrical conductivity, redox behaviour, ease of preparation, adaptability for modifications, and environmental stability.[66,110–112] It can be synthesized by different methods as described below with their respective advantages and disadvantages mentioned in Table 1.

3.1. Vapor-phase polymerization

Vapor-phase polymerization comes under the self-assembly polymerization technique and is used for the preparation of very thin polymer films like PANI, polypyrrole, and polythiophene (Fig. 2a). This method produces polymers with high purity and superconductivity, at nano-scale levels.[133] This method was used to deposit conductive PANI using polyacrylamide in 1998, by saturating it with ammonium peroxydisulfate; subsequently, casting this film on a glass plate, which underwent vacuum drying for 48 h at 50 °C; and subjected to HCl treatment, followed by aniline vapor.[134] In general, it is a simple closed chamber setup where the oxidant is applied through the solvent coating and then exposed to the coated surface to aniline monomer vapor.[135] Kim *et al.*[133] reported the synthesis of PANI nanofilms by the vapor phase deposition method on polymeric substrates like polyethylene terephthalate (PET), polyimide (PI), polyvinyl chloride (PVC), and polystyrene (PS), which involved coating the substrates with 10 wt% oxidant solution (ferric chloride, camphor sulfonic acid (CSA), and Fe *para*-toluenesulfonate in methyl alcohol) through dip- or spin-coating. Thereafter, dry-coated films were exposed to aniline vapor in a reaction chamber at a controlled temperature between 50 °C and 80 °C for 5 to 60 min. Finally, the films were washed with methanol to remove the unreacted substances and dried at 80 °C. In addition, Gao *et al.*[136] used this method to synthesize PANI by placing an aniline monomer and a mixture of HCl and ammonium persulfate (APS) in a sealed glass container comprising a plastic membrane with few holes (dia. = 0.1 cm) to reduce the polymerization rate. This membrane regulates the contact and reaction of the reactant vapors, ensuring a slower polymerization process. The vapor-phase polymerization method has successfully been used to prepare crystalline PANI with dendritic structures.[136]

3.2. Photoinduced polymerization

This photochemical polymerization method is used for the synthesis of conducting PANI or its derivatives in different studies.[133,137,138] Moreover, some studies have used different ranges of light for synthesis. For instance, Gizdavic-Nikolaidis *et al.*[139] used microwave radiation, and Felix *et al.*[140] utilized X-ray irradiation (Fig. 2b). Ishioka *et al.* synthesized PANI using neodymium-doped yttrium aluminum garnet (Nd:YAG) laser to irradiate on Au electrode in a solution containing aniline under an applied external bias.[110,141] PANI could be synthesized through the photo-polymerization process using single or bi-layer films containing $[Ru(bipy)_3]^{2+}$ as a primer and methylviologen (MV^{2+}) as an oxidizer. These components worked together to facilitate the controlled polymerization of aniline. When irradiated with visible light at a wavelength of 452 nm, $[Ru(bipy)_3]^{2+}$ transitioned into a highly reactive triple excited state $*[Ru(bipy)_3]^{2+}$. This state enabled the e^- transfer between $*[Ru(bipy)_3]^{2+}$ and MV^{2+}, thus producing $[Ru(bipy)_3]^{3+}$, which is a powerful oxidizing agent that plays a crucial role in oxidizing aniline molecules, ultimately leading to their polymerization into PANI.[87,138,142] The synthesized PANI got deposited on the single or bi-layer films, making it ideal for application in electronics, which require thin- and conducting-film polymer layers.[87] This method also leads to the formation of composite materials where the formation of nanowires and microwires of silver occurs.[110] The morphology of the obtained polymer is majorly dependent on the wavelength of the light source, such as a globular structure upon UV light irradiation and a fibrillar structure upon visible light irradiation.[110]

3.3. Chemical polymerization

The chemical polymerization process is extensively utilized due to its simplicity, cost-effectiveness, and ease compared to other methods for synthesizing PANI.[86] This method undergoes chemical oxidation which involves the combination of a monomer, an oxidizing agent, and an acid under ambient conditions[96] (Fig. 2c). The commonly used oxidizing agents include APS,[143–147] ceric nitrate, cerium (IV) sulfate,[148,149] sodium vandate, hydrogen peroxide,[150] potassium iodate,[151,152] and potassium dichromate.[153,154] Oxidative polymerization is conducted in an acidic

Open Access Article. Published on 12 February 2026. Downloaded on 3/23/2026 6:55:17 AM.
This article is licensed under a Creative Commons Attribution 3.0 Unported Licence.

Table 1 Different methods for the synthesis of PANI

Methods	Precursors	Synthesis conditions	Morphologies	Advantages	Disadvantages
Electrochemical polymerization[113–118]	Aniline, camphor sulfonic acid (CSA), DI water, ITO glass substrate as electrode, an ultra-grade stainless steel electrode, ethanol, acetone, and stainless steel electrode	Electrode dimensions = 2 cm × 7.5 cm; electrode gap = 1 cm; area of electrode immersed = 12 cm^2 and room temperature	Film	Accurate regulation on the PANI properties; mild reaction conditions; capability to modify the polymer structure; ease of doping during synthesis; better reproducibility and eco-friendly process	Requires energy input; restricted scalability; necessity for specialized apparatus and issues with electrochemical stability
	Aniline, CSA, ITO-coated glass substrate, an ultra-grade stainless steel electrode, DI water, ethanol, and acetone	Electrode dimensions = 2.5 cm × 2.5 cm; electrode gap = 1 cm; area of electrode immersed = 5 cm^2; temperature = 25 °C and constant potential of 1.5 V was applied for 60 s	Fibre-like morphology		
	Aniline, H_2SO_4, ITO electrode, copper foil (0.5 cm × 1.5 cm), and DI water	Potential = +3 V for 30 min and room temperature	Homogenous film		
	Na_2SO_4, H_2SO_4, aniline, stainless-steel sheets, deionized water and ethanol, a saturated calomel electrode, small segment of stainless steel, and NaOH	Time = 1800 s for variable potential ranges, temperature = 60 °C, and dried in an oven	Agglomerated flakes (1.3 V) and spongy structures (>1.3 V)		
	Working electrode – (FTO plate) with 1 cm diameter and 3 cm length, stainless steel as the counter electrode, and Ag/AgCl as the reference electrode, aniline, and H_2SO_4	20 Cycles, sweep speed = 0.05 V s^{-1}; potential window = −0.2 V to 1.0 V; product: Dried in an oven at a temperature of 60 °C and time = 24 h	Disordered and porous arrangement, made up of granules and fibers		
Chemical polymerization[118–126]	Aniline, double-distilled water, dodecylbenzenesulphonic acid (DBSA), $FeCl_3 \cdot 6H_2O$, and acetone	Stirred for 12 h and dried in an oven at 60 °C for 24 h	Cauliflower-like surface morphology	Easy, fast and straightforward method; PANI with high purity can be obtained; precise control over doping and morphology and potential for industrial scale production	Involves toxic chemicals, including oxidizing agents; controlling thickness of the polymer is very difficult and severe reaction conditions
	Aniline, HCl, ammonium persulfate (APS), DI water, and ethanol	Time = 3 h for stirring and drying at a temperature of 60 °C	Nanorods		
	$(NH_4)_2S_2O_8$, aniline, phytic acid, DI water and ethanol	Reaction temperature = 4 °C; removal of soluble components; hydrogel was soaked in 500 mL DI water for 1 day and vacuum drying at a temperature of 60 °C	Nanorods		
		Mixture was stirred in an ice water bath at 0 °C for 6 h; time	Irregular spherical morphology		

© 2026 The Author(s). Published by the Royal Society of Chemistry

Open Access Article. Published on 12 February 2026. Downloaded on 3/23/2026 6:55:17 AM.
This article is licensed under a Creative Commons Attribution 3.0 Unported Licence.

Table 1 (*Contd.*)

Methods	Precursors	Synthesis conditions	Morphologies	Advantages	Disadvantages
	Aniline, HCl, ammonium persulfate, and ultra-pure water	= 24 h; dried at a temperature of 60 °C			
	Aniline, HCl, APS, and acetone	Rapid mixing for 30 s; reaction time = 2 h and product vacuum dried at 60 °C for 12 h	Nanofibres		
Vapor-phase polymerization[97,100,127,128]	Oxidants like $FeCl_3$, camphorsulfonic acid and Fe(III) *p*-toluenesulfonate prepared in methylalcohol (MeOH), polymeric substrates coated with oxidants, aniline vapor, and methanol	Exposed to aniline vapor for 5–60 min in a reaction chamber under several temperatures and PANI were dried for 3 min at 80 °C	Nanofilms	High-purity product having excellent conductivity; uniform polymer film deposition and forms thin films having a smooth surface	Complex equipment requirement and weak interaction between material components
	Aniline, HCl, ammonium persulfate (APS), sealed glass container, and plastic membrane with many needled holes with an average diameter of about 0.1 cm	Reaction temperature: 0–5 °C	Dendritic structures		
	Fe(III) tosylate in a 40% aqueous solution of ethanol, aniline, 3 electrode cells, and methanol	Electrode surface: 250 μL of Fe(III) tosylate solution drop-casted; heated at 120 °C for ~3 min; electrode placed ~6 cm from the aniline reservoir in a sealed chamber; exposed to aniline vapor for 1 h at room temperature (not under vacuum) and electrode washed with methanol; dried under a hot air blower (40 °C) for ~20 s	Interconnected nanofibres		
Photopolymerization[101,103,104,129]	Ammonium hydroxide, aniline, nitric acid, acetonitrile, HCl or H_2SO_4, ultra-pure water, plastic cuvette (with a 1 cm optical path), X-ray irradiation, and Cu anode	X-ray wavelength = 0.1541 nm with a voltage of 30 kV and a current of 40 mA	Fibrillar morphology	Thickness of the polymer can be controlled; size and shape can be controlled and porous structure can be synthesized	Low yield; needs light source and cannot be utilized for every polymer
	Aniline, potassium iodate, HCl, and microwave	MW operating at 2.45 GHz; absorbed power = 6.6 ± 0.4 W for 93 W emitted power; reaction temperature = 24 °C ± 1 °C; time = 20 min and yield = 78.8%	Nanofibers		

Open Access Article. Published on 12 February 2026. Downloaded on 3/23/2026 6:55:17 AM.
This article is licensed under a Creative Commons Attribution 3.0 Unported Licence.

Table 1 (*Contd.*)

Methods	Precursors	Synthesis conditions	Morphologies	Advantages	Disadvantages
	2-2-Dimethoxy-2-phenylacetophenone (DMPP), aniline, ethylene glycol dimethacrylate (EGDMA), and ultraviolet light	Reaction time = 600 s and under continuous nitrogen gas flow	—		
Enzyme-catalysed polymerization[130–132]	Aniline, HRP, hydrogen peroxide, and phosphate buffer	Room temperature; vigorous stirring and pH = 3		Environment friendly and minimal purification and separation are needed	Slow reaction; branched polymeric materials and non-conducting forms
	Aniline, sulfonated polystyrene (SPS), hydrogen peroxide, HRP, and sodium phosphate	pH = 4.0 and time = 3 h	—		

medium (pH < 3) for dissolving aniline, initiating polymerization, and minimizing the unwanted by-product such that it gives polymers with strong conductivity.[155] The temperature of the solution affects the outcome and is maintained between 0 °C and 4 °C, as it influences the conductivity and viscosity of the resulting PANI.[156] The quantity of oxidant also impacts the polymerization as it can degrade the polymer if the quantity is kept high. Moreover, ammonium and alkaline salts may be used sometimes as buffers as they influence the quality, yield, and conductivity of PANI.[59] The chemical polymerization of aniline using an oxidant in an acidic solution is nearly similar to that of the electrochemical polymerization of aniline in terms of reaction kinetics.[157] The initial step of the reaction involves APS capturing the e^- from the nitrogen atom of the aniline to form an aniline radical cation.[86] Polymerization starts with the proton elimination from aniline monomers by oxidants, leading to the formation of its radical cation. Further, the nitrogen radical cation adds up at the para position of another aniline molecule, forms a bond, and then promotes the continuous growth of polymer chains. The para position discussed is the primary pathway; however, in certain instances, reactions may occur at the ortho position. This can lead to structural irregularities or distortions in the resulting PANI, ultimately affecting the uniformity and properties of the polymer.[158] Dan and Sengupta[159] suggested that the reaction yield and intrinsic viscosity of the polymer are influenced by the synthesis parameters. Erdem *et al.*[160] examined the effects of different acids and oxidants on the polymerization of PANI. The yield and conductivity of PANI were observed to follow the descending order: oxalic acid > malonic acid > succinic acid > glutaric acid > adipic acid > phthalic acid. Blinova *et al.*[161] examined the chemical oxidative polymerization by varying the oxidant (APS)-to-monomer (aniline) molar ratio in an acidic medium (HCl). The polymerization yield showed an increase with the molar ratio of oxidant to monomer ranging from 0.2 to 1.5.[66]

3.4. Enzyme-catalyzed polymerization

The enzyme-catalyzed method is environment-friendly and uses oxidoreductase catalytic enzymes like horseradish peroxidase (HRP), soybean peroxidase, bilirubin oxidase, laccase, and glucose oxidase. These enzymes facilitate the oxidation of aromatic amines and phenols during polymer synthesis, with oxidants like peroxide, which ultimately transforms into water (Fig. 2d).[130,162,163] To address issues related to branched polymers, Samuelson *et al.*[130] used various electrolytes including polystyrene sulfonate (PSS) as templates in the HRP for the catalyzed PANI with regular polymeric chains. The polymerization process occurs in an acidic medium at pH 4 to form water-soluble PANI.[164] It may be noted that PSS plays a definite role in the synthetic process: it acts as a template that aligns aniline monomers during polymerization, facilitating *para*-directed, head-to-tail coupling of the aniline units.[87] In addition, PSS acts as a dopant in activating PANI to form an electrically conductive EM salt and imparts water solubility to the product. This polyanion-assisted polymerization allows the enzymatic synthesis of the water-soluble complex of conducting PANI with

 © 2026 The Author(s). Published by the Royal Society of Chemistry

Open Access Article. Published on 12 February 2026. Downloaded on 3/23/2026 6:55:17 AM.
This article is licensed under a Creative Commons Attribution 3.0 Unported Licence.

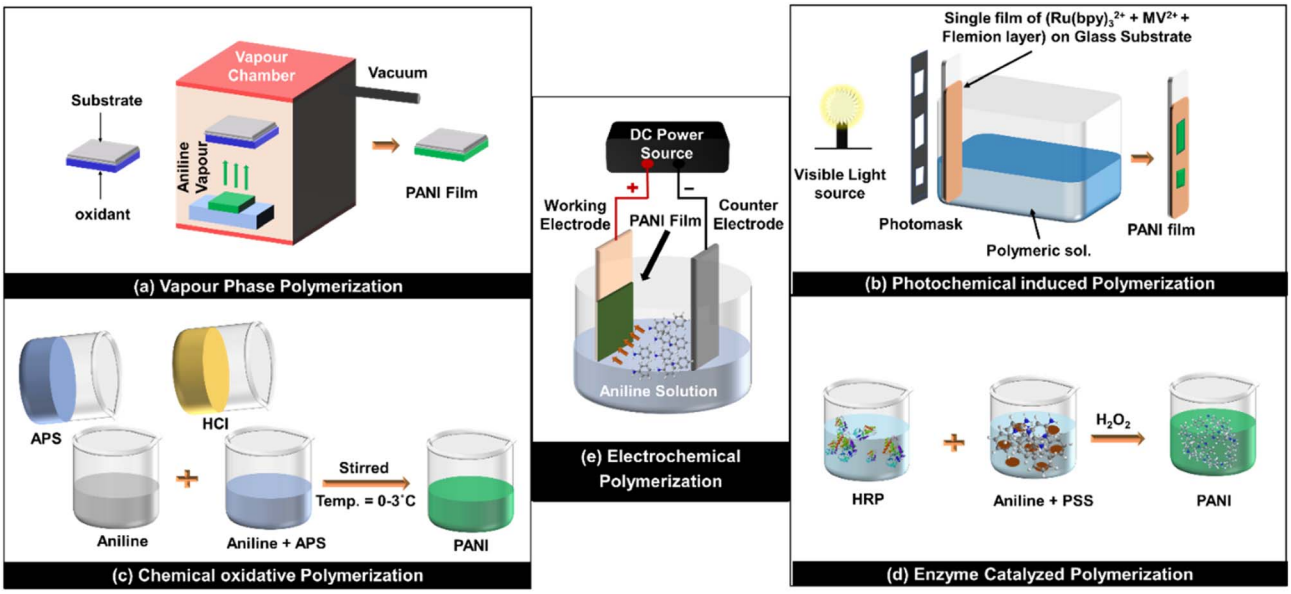

Fig. 2 Schematic of the synthesis methods of PANI *via* (a) vapor-phase polymerization, (b) photochemical induced polymerization, (c) chemical oxidative polymerization, (d) enzyme-catalysed polymerization, and (e) electrochemical polymerization (abbreviations: PANI – polyaniline, APS – ammonium persulphate, HCl – hydrochloric acid, PSS – polystyrene sulfonate, HRP – horseradish peroxidase).

a well-defined structure at pH of 4.3.[165–167] However, the higher degree of complexity between PANI and the polyanion makes it difficult to obtain bulk PANI required for specific purposes, such as the formation of free-standing films and fibers.[165] This approach is straightforward and environmentally sustainable, involving a one-step polymerization process under mild conditions that necessitate minimal or no additional purification.[130]

Enzyme-catalyzed polymerization also utilizes surfactant micelle templates to guide polymer chain growth by creating an acidic environment (low pH) and preventing unnecessary branching.[164,168] The dry-spinning technique in enzyme-catalyzed polymerization enhances the processability of enzymatically synthesized PANI, producing fibers with improved tensile strength, conductivity, and crystallinity due to chain alignment.[169] In addition, enzyme immobilization on PANI nanotubes enhances electrocatalytic performance, with smaller nanotubes of size approximately 100 nm, showing the highest catalytic currents due to greater surface area and conductivity.[131]

3.5. Electrochemical polymerization (ECP)

The ECP method is mainly employed in the preparation of pure PANI with thin film morphology (Fig. 2e). The nanostructured PANI having a thin film morphology provides a high specific surface area, making it suitable for various applications. The ECP reaction offers a better way to polymerize, allowing precise control over the beginning and last steps of the process. Electrochemical reactions are usually cleaner, and the resulting PANI is purer ascribed to the electrochemical polymerization, which does not involve the addition of any oxidant, surfactant, or other additional chemicals.[110,113] This method for preparing PANI involves the following steps: formation of positive free radicals of aniline monomers by the oxidation at the anode; the formation of the dimers through the process of removing protons; rearranging e^- in the aromatic rings; growth of dimers and formation of the new structure; and spontaneous activation of the polymeric chain formed by acids present in the solution.[80,87,158]

The ECP method is typically employed for polymerization *via* three main ways, namely galvanostatic, potentiostatic, and potential cycling or potentiodynamic means.[79,170–173] In the first method, a 2-electrode setup is immersed in an electrolyte containing monomers, and a specific current is applied to form a PANI film on a Pt foil electrode.[110,174] The controlled flow of current ensures stable and precise deposition of polymers.[79,172] In the potentiostatic method, the current is varied, but the potential of the electrodes is kept controlled. This process forms a polymer powder that weakly adheres to the electrode.[175,176] When aniline undergoes electro-oxidation through continuous cycling between the decided potentials, it leads to the formation of a smooth and adhering polymeric film on the electrode surface. The characteristics of PANI film can be adjusted accordingly in terms of conductivity by oxidation or reduction.[177,178] In the potentiodynamic method, the potential is kept cycling between the minimum and maximum potential limits in the cycle. This facilitates the layer formation of polymers, and the previous layer also gets activated before the next layer gets deposited.[179–181] The amount of deposition in the potentiodynamic method depends on the sweep rate, and the quantity of deposition in each sweep decreases with the increase in its rate. Moreover, the porosity of the so-formed PANI increases with the increase in sweep rates.[180] In addition, there is a continuous polymerization process that occurs in galvanostatic and potentiostatic, but this growth process gets interrupted between the two successive sweep cycles in the case of the potentiodynamic method. It is noteworthy that electrochemical deposition

Open Access Article. Published on 12 February 2026. Downloaded on 3/23/2026 6:55:17 AM. This article is licensed under a Creative Commons Attribution 3.0 Unported Licence.

is a rapid, easy, and clean method resulting in a highly conductive nature.[111]

4. Components to be integrated to form PANI-based composites

PANI is characterized by its unique structure containing amine and imine groups, which contribute to its electrical and chemical properties. These combined characteristics make PANI a multifaceted material for many applications, especially in photocatalysis. PANI acts as an efficient e^- donor and transporter of photogenerated h^+ in the presence of visible light, which enhances the photocatalytic efficiency, owing to rapid charge carrier migration.[182–185] It exhibits excellent chemical stability and functions across a wide pH range, maintaining both performance and structural integrity under acidic and basic conditions.[186] Various PANI-based composites have been synthesized to leverage the aforementioned merits. In addition, PANI nanocomposites are synthesized by combining PANI with other components such as metal oxides, metal ferrites, metal sulfites, metal halides, carbonaceous compounds, organic compounds, inorganic compounds, and metalloids.[187–191]

4.1. Metal oxides

Metal oxides have been widely used as photocatalysts due to their unique properties, making them highly suitable for environmental remediation and energy conversion applications.[192–198] Their high surface area, nanoparticle size, and unique physical and chemical characteristics enhance their capacity to adsorb and degrade toxic contaminants.[193,199] In this regard, several metal oxides such as TiO_2, ZnO, ZrO_2, Fe_2O_3, γ-Fe_3O_4, SnO_2, Mn_2O_3, WO_3, CeO_2, CuO, and NiO have been widely used in the area of environmental remediation.[200,201] Despite their good light-harvesting capabilities, metal oxides face several limitations, including a wide bandgap that restricts absorption to the UV region, high e^-/h^+ recombination rates that reduce photocatalytic efficiency, and susceptibility to photocorrosion, which compromises stability and reusability.[202–207] Further, to overcome these shortcomings, metal oxides have been integrated with PANI.[208–212] Such composites of PANI with metal oxides reduce their optical E_g and shift the absorption peak from UV to the visible region. This consequently leads to the enhanced photocatalytic property of metal oxide/PANI composite attributed to leveraging the e^-/h^+ separation and photosensitization property of PANI, influencing the contaminant degradation efficiency.[210,212,213] Additionally, PANI adsorbs negatively charged organic and inorganic dyes due to the protonation of its imine group, hence possessing a positive surface charge. Such electrostatic interaction results in strong and stable adsorptive removal of dyes.[17,214] A PANI/magnetic oxide composite was synthesized for the degradation of methylene blue (MB) dye, achieving a photocatalytic efficiency of 99%. This high performance is attributed to the uniform dispersion of iron oxide nanoparticles within the PANI matrix and on its surface, resulting in a synergistic interaction between the iron oxide and PANI phases.[215] The PANI/Sn_3O_4 composite was prepared for the removal of Rhodamine B (RhB) dye, achieving a removal efficiency of approximately 97%. The composite exhibited 2.27 times higher photocatalytic activity under visible light compared to pure Sn_3O_4.[216] A TPU/TiO_2/PANI membrane was synthesized for the photodegradation of Congo red (CR) dye and the reduction of Cr(VI), achieving efficiencies of 99.7% in 30 min and 99% in 25 min, respectively, under visible light. These values were 2.1 and 3 times higher than those obtained with the TPU/TiO_2 membrane.[217]

4.2. Metal sulfides

Metal sulfides have gained prominence as photocatalysts due to their ease of synthesis, low cost, efficient charge separation, and narrow E_g, which enable effective visible light utilization and strong reducibility, supporting redox reactions beneficial for environmental remediation.[218–220] In recent years, various metal sulfides including CuS,[221–226] ZnS,[227] CdS,[228–236] NiS_2,[237] MoS_2,[238–241] In_2S_3,[242–244] $ZnIn_2S_4$,[245,246] and $Zn_xCd_{1-x}S$[247] have been used as photocatalysts. Despite their many advantages, metal sulfides face several challenges in photocatalysis, including low stability, high charge-carrier recombination rates, limited light absorption intensity, and susceptibility to photocorrosion.[218,230,231,248–250] In this context, metal sulfides can be combined with PANI to overcome the aforementioned demerits, thereby enhancing the photocatalytic efficiency.[251] A Ag-doped ZnO–ZnS/PANI composite is synthesized for the degradation of the persistent organic pollutant MB dye. The incorporation of PANI into Ag-doped ZnO–ZnS enhanced the photocatalytic degradation efficiency from 72% to 95% under UV light. This improvement is attributed to strong interfacial coupling, which facilitated efficient electron transfer from PANI to Ag *via* the ZnO–ZnS matrix, leading to the generation of superoxide ($^{\bullet}O_2^-$) and hydroxyl ($^{\bullet}OH$) radicals.[252] ZnS/CdS/PANI has been prepared for the removal of anionic and cationic dyes in which after the addition of PANI, the degradation rate of RhB increases from 81.1% to 96.5%. It is suggested that the sensitization of ZnS/CdS with PANI decreases the recombination of photogenerated carriers and increases the specific surface area and efficiency of electron–hole pair separation.[189]

4.3. Metal ferrites

Metal ferrites are compounds composed of magnetic materials having iron oxide combined with metals Mn, Ni, Zn, Cu, La, *etc.*, exhibiting magnetic properties, chemical stability, and photocatalytic efficiency, which are helpful in environmental remediation. Metal ferrites are extensively applied for the reduction of heavy metals and the adsorption of CO_2.[253–255] The properties of ferrites are mainly influenced by their nature, site, and the amount of metal added to the structure.[256] The addition of cations like Mg^{2+},[257] Zn^{2+},[258] and Al^{3+} (ref. 259) improves the stability of ferrites.[256] Along with it, the addition of transition metals like Ni^{2+}, Cu^{2+},[259] Mn^{2+},[260] and Co^{2+} (ref. 261) in the spinel lattice significantly alters their redox properties and also the moment of nanoparticles affecting magnetic properties.[256,262] These ferrites exhibit excellent adsorptive capacity in wastewater treatment and degradation of dyes, pharmaceuticals, and other contaminants because of their ability to absorb

 © 2026 The Author(s). Published by the Royal Society of Chemistry

Open Access Article. Published on 12 February 2026. Downloaded on 3/23/2026 6:55:17 AM. This article is licensed under a Creative Commons Attribution 3.0 Unported Licence.

light and exhibit photocatalysis.[263–266] Despite their advantages, metal ferrites have a high recombination rate of e^-/h^+ pairs, which decreases the efficiency.[264] Moreover, some metal ferrites have low surface areas that affect the active sites facilitating photocatalysis.[267–269] Ag/$CoFe_2O_4$/PANI was synthesized by Mosali *et al.*[270] for the removal of MB dye, and the proposed mechanism of photocatalysis states that PANI played a crucial role in absorbing the visible light and generating electrons to be transferred from the HOMO level to the LUMO level and facilitated the transfer of e^- to the CB of $CoFe_2O_4$, which enhanced the overall photocatalytic efficiency. Additionally, methyl orange (MO) and RhB are removed in a study conducted by Li *et al.*[271] utilizing $ZnFe_2O_4/TiO_2$/PANI with 98% degradation efficiency, attributed to the property of PANI to donate e^- and accept h^+ after the irradiation of light, enhancing the charge separation efficiency.

4.4. Carbonaceous materials

Conventional carbonaceous materials such as graphenes, graphite, activated carbon, fullerenes, carbon nanotubes, carbon black, and graphitized materials have long been used in the field of heterogeneous catalysis. Their unique properties such as high surface area and versatility enable them to function as both direct catalysts and support materials.[272,273] Graphene consists of a single layer of carbon atoms arranged in a hexagonal or 2D honeycomb structure.[274,275] When graphene layers are rolled in cylindrical shapes at specific angles, it leads to the formation of carbon nanotubes (CNTs). CNTs possess a remarkably high surface-to-volume ratio and demonstrate outstanding thermal, electrical, and mechanical properties, which are influenced by the angle of graphene rolling and the cylinder's diameter.[276,277] Graphene-based materials such as graphene oxide (GO) and reduced graphene oxide (rGO) have been widely studied for wastewater treatment.[278,279] This material possesses high surface area, tunable pore size, good conductivity, and excellent surface chemistry, enabling them to be effective in the adsorption and photodegradation of pollutants like dyes,[280,281] PPCPs,[282] heavy metals,[283] phenols,[284,285] and pesticides.[286] The unique chemical and physiochemical properties of GO and rGO resulting from the functional groups like epoxy, hydroxyl, carboxyl, and carbonyl provide better adsorption efficiency in the removal of water pollutants.[287,288] Despite their merits, carbonaceous materials also face several challenges, including limited affinity for anionic dyes and heavy metals, slow and inefficient material recovery, and reduced adsorption efficiency due to the aggregation of GO sheets.[289] Several studies have shown enhanced photocatalytic properties by combining CNTs, GO, and rGO with PANI. According to the literature, a ZnO/rGO composite achieved 87% degradation efficiency of MB dye in 130 min under UV light. In comparison, a ZnO/rGO/PANI ternary nanocomposite exhibited 99% efficiency in the removal of MO within just 60 min under UV irradiation.[290] This phenomenon is linked to PANI, which improves light absorption and increases the material's surface area, while rGO significantly boosts the transfer of photogenerated charge carriers. PANI/RGO demonstrated significantly enhanced photodegradation capabilities compared to the individual materials, achieving over 98% removal efficiency for both cationic and anionic dyes such as malachite green, RhB, and Congo red. Additionally, it reduced Cr(VI) by 94.7% within just 15 min.[291] Ag_3PO_4@MWCNTs@PANI showed excellent photocatalytic activity under visible light, degraded both phenol and *p*-nitrophenol with 100% efficiency within 20 min, which is 21.9 and 10 times higher than that of bare Ag_3PO_4, respectively, where PANI acted as a h^+ transporting material with low recombination and fast charge separation and the MWCNT served as a photogenerated charge electrode.[292]

5. Synthesis of PANI-based ternary photocatalysts

5.1. Chemical precipitation method

In this method of composite preparation, a pre-synthesized binary composite comprising PANI as one of its components is incorporated with the third component *via* the chemical precipitation method. Moreover, this method is facile and cost-effective, and can be carried out under mild conditions. For example, Selvin *et al.*[293] reported the synthesis of a ZnO/activated charcoal/PANI nanocomposite through this method. To 0.05 g of pre-synthesized activated charcoal/PANI binary composite, 0.1 M zinc acetate dihydrate was added and stirred at 70 °C, followed by the addition of 0.2 M NaOH to fabricate the ternary composite ZnO/activated charcoal/PANI. Similarly, Hu/PANI@Ni_2O_3 was synthesized by adding an aqueous solution of nickel (II) nitrate hexahydrate to a previously prepared 8% (w/v) Hu/PANI suspension. Subsequently, an alkaline hypochlorite solution was gradually added, and the mixture was stirred vigorously for 2 h at room temperature. This led to the precipitation of a solid, which was then collected, thoroughly washed, and dried in a hot air oven. The final product was referred to as Hu/PANI@Ni_2O_3 (Fig. 3a).[294] In another study, Qing *et al.*[295] reported the encapsulation of PANI fibers by β-cyclodextrin (β-CD@PANI), which effectively inhibits the recombination of photoinduced charge carriers. To further enhance the photocatalytic performance, BiOBr was introduced into the as-synthesized binary composite to form C-PANI/BiOBr, thereby extending its light absorption capability compared to bare BiOBr. The ternary composite was prepared by first adding 4.5 mL of acetic acid to a bismuth(III) nitrate pentahydrate solution, followed by stirring for 2 h. Subsequently, KBr and sodium acetate (CH_3COONa) were added, resulting in a solution of pH 2.8. Interestingly, at this pH, the two components carried opposite charges: C-PANI exhibited +13.9 eV, while BiOBr showed −6.2 eV. Based on this electrostatic potential difference, the final solution was maintained at room temperature for 12 h to facilitate electrostatic interaction. The resulting product was then separated, washed, and dried at 60 °C to obtain the desired C-PANI/BiOBr (Fig. 3b).

5.2. *In situ* polymerization

Unlike the chemical precipitation method, *in situ* polymerization involves the addition of the as-synthesized binary

Open Access Article. Published on 12 February 2026. Downloaded on 3/23/2026 6:55:17 AM.
This article is licensed under a Creative Commons Attribution 3.0 Unported Licence.

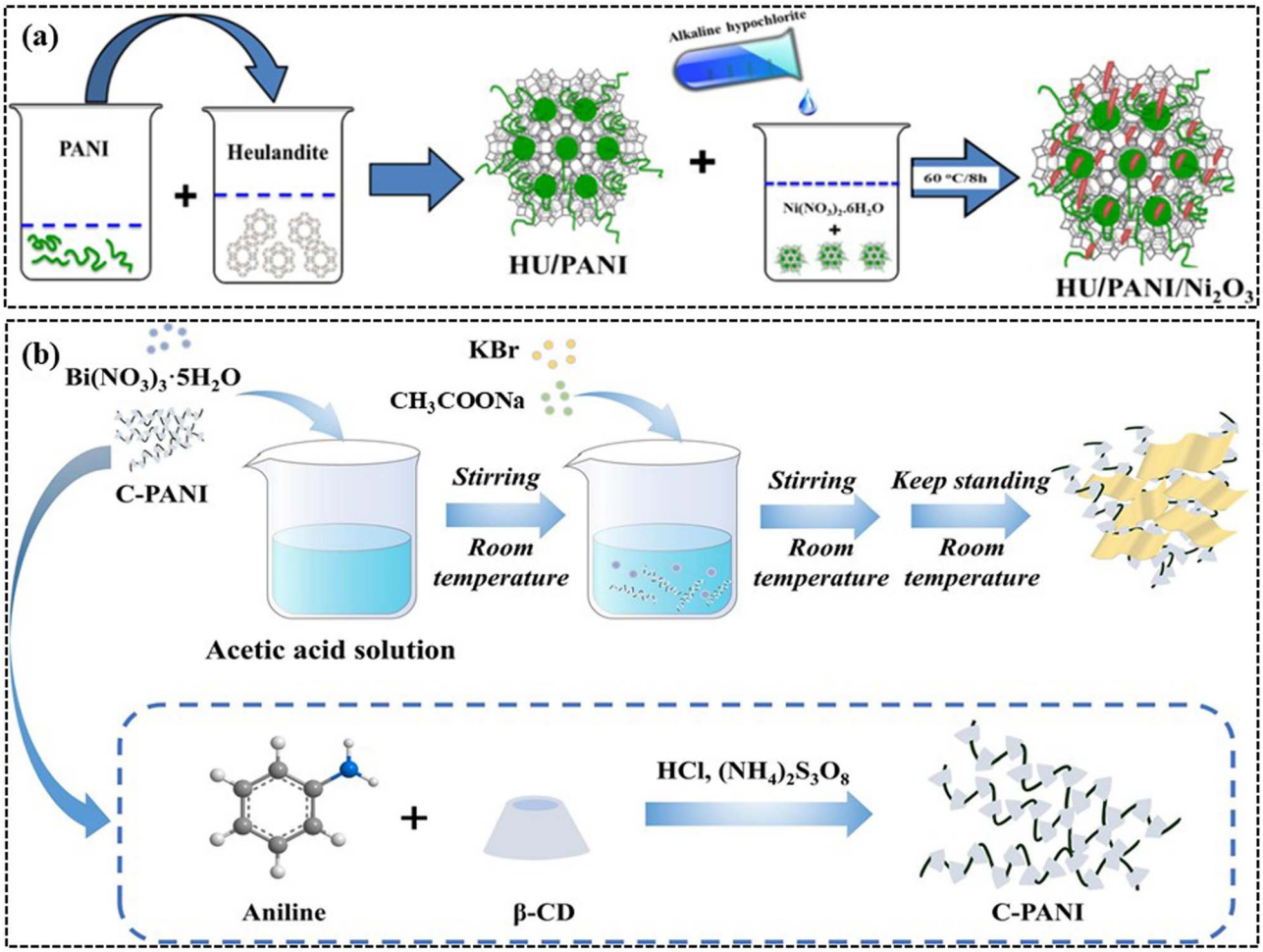

Fig. 3 Schematic of the synthesis of the PANI-based ternary composite using chemical precipitation: (a) Hu/PANI@Ni_2O_3 (reproduced from Abukhadra *et al.*, 2018 (ref. 294) (Open Access) and (b) C-PANI/BiOBr (modified and reproduced with permission from Qing *et al.*, 2023 (ref. 295)).

composite (excluding PANI) during the fabrication of a PANI-based ternary photocatalyst. Particularly, the binary composite is added to an acidic solution containing an aniline monomer, followed by the systematic addition of an oxidant, such as APS, to initiate polymerization under continuous stirring. The *in situ* polymerization process involves the polymerization of pure monomer molecules over the selected pre-synthesized nanomaterial.[66] For instance, while preparing PANI by adding equimolar amounts of aniline and HCl, Shankar *et al.*[296] introduced finely ground rGO and carbon-doped porous ZnO (C–ZnO) into the mixture and stirred it for 30 min. The resulting suspension was then transferred to an ice bath, followed by the dropwise addition of 1 M APS under continuous stirring, which produced a magenta color. The subsequent appearance of a green complex indicated the formation of EM, confirming the successful synthesis of the rGO-PANI-assisted C–ZnO nanocomposite. Furthermore, the reported procedure is illustrated in Fig. 4a.

In another study, Liu *et al.*[298] fabricated PANI-coated TiO_2/SiO_2 (P/TS) by integrating electrospinning, calcination and *in situ* polymerization. Initially, the TiO_2/SiO_2 (TS) nanofiber membrane was pre-treated with acetone, ethanol, and deionized (DI) water to enhance its hydrophilicity before PANI coating. In an ice bath, the conditioned TS membrane was immersed in an aniline solution, followed by the addition of 1 M HCl and 15 mL APS, resulting in a solution with a 1 : 2 molar ratio of APS and aniline, thereby facilitating the formation of an EM salt coating on the TS nanofiber. Additionally, to remove residual oligomers, the as-prepared P/TS nanofiber was adequately washed with HCl, rinsed with DI, and dried at 40 °C. In a study, Shoueir *et al.*[297] fabricated a guanine-based bio-MOF (ZnONPs/MOF), which was subsequently dispersed in a solution containing aniline hydrochloride, HCl, and DI water using ultrasonication. A mixture of 0.22 g of APS and 2 mL of HCl was then added to the dispersion, and the pH was adjusted to 2.5. Thereafter, the solution was placed in an ice bath for 10 h to complete the polymerization reaction, resulting in a dark greenish solution. This product was thoroughly washed with DI water/ethanol to remove residual chloride ions and excess APS. Unlike the previous study, the final product was treated with ammonium hydroxide, increasing the pH to 10 and facilitating deprotonation. The composite was then vacuum-dried at 80 °C

 © 2026 The Author(s). Published by the Royal Society of Chemistry

Open Access Article. Published on 12 February 2026. Downloaded on 3/23/2026 6:55:17 AM.
This article is licensed under a Creative Commons Attribution 3.0 Unported Licence.

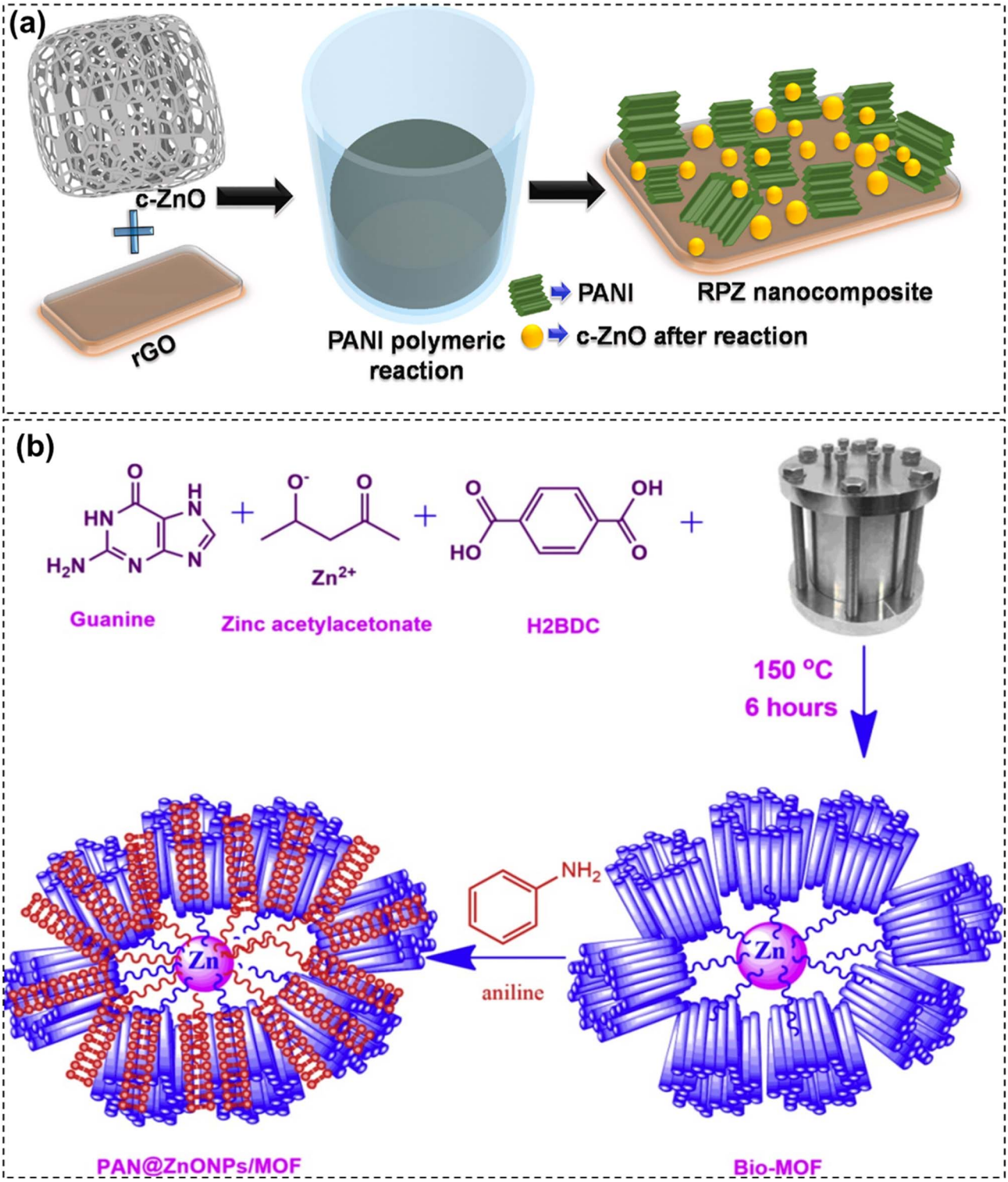

Fig. 4 Schematic of the synthesis of the PANI-based ternary composite using *in situ* polymerization: (a) RPZ composite (reproduced with permission from Shankar *et al.*, 2021 (ref. 296)) and (b) PAN@ZnONPs/MOF (reproduced with permission from Shoueir *et al.*, 2020 (ref. 297)).

for 24 h to obtain the PAN@ZnONPs/MOF material. The overall synthesis process is illustrated in Fig. 4b. However, Wang *et al.*[299] synthesized rGO/CuI/PANI *via* a self-assembly approach. Initially, Cu^{2+} ions were immobilized on the surface of GO using a water bath at 60 °C. The resulting Cu^{2+}–GO was collected and again dispersed in a KI solution. Subsequently, aniline was added, and the mixture was stirred for 8 h, leading to the polymerization of aniline into PANI on the Cu^{2+}–GO surface. The resulting black precipitate was then collected, rinsed, and vacuum-dried to yield the rGO/CuI/PANI composite.

Open Access Article. Published on 12 February 2026. Downloaded on 3/23/2026 6:55:17 AM.
This article is licensed under a Creative Commons Attribution 3.0 Unported Licence.

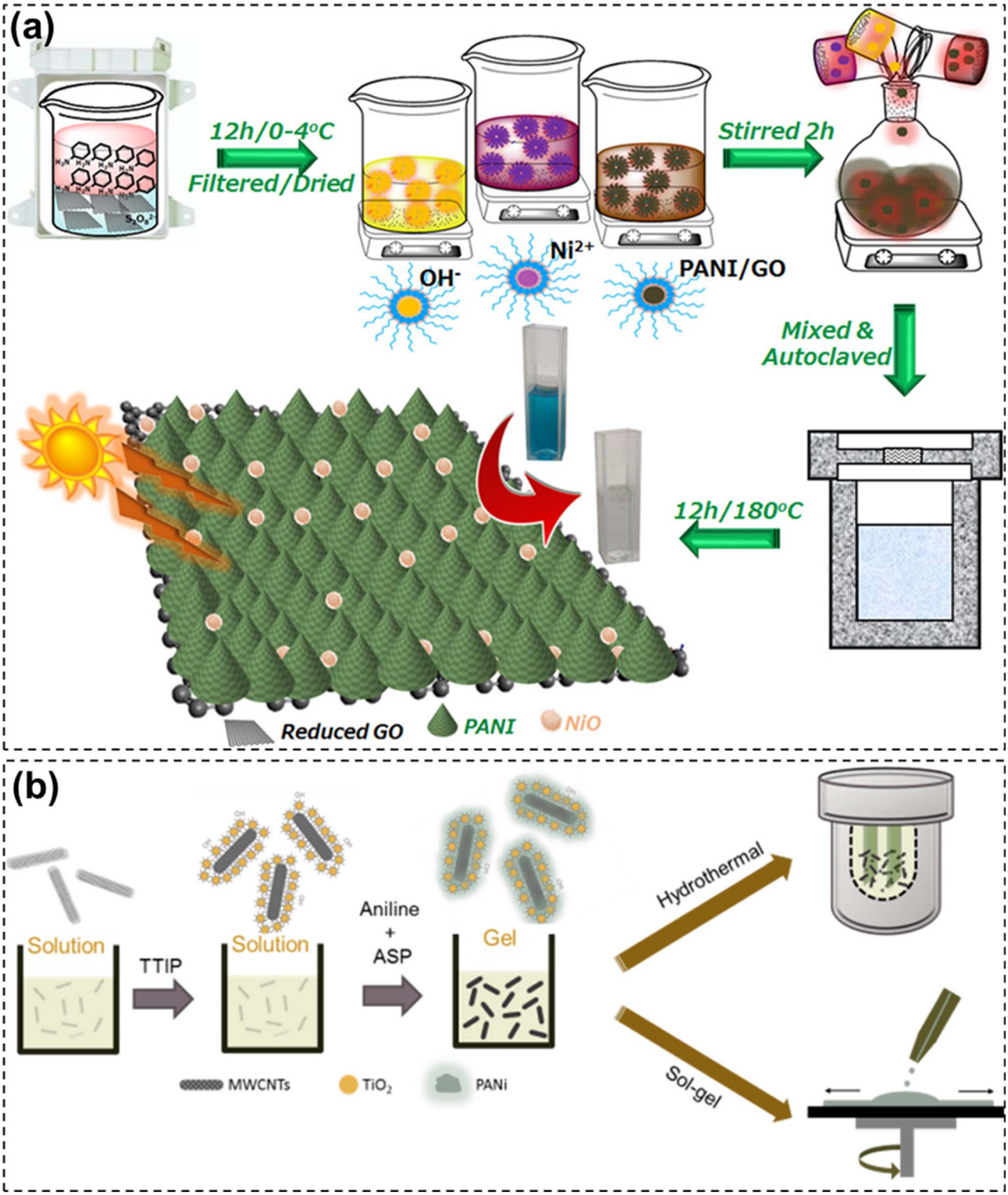

Fig. 5 Schematic of the synthesis of the PANI-based ternary composite using the solvothermal method: (a) NiO@PANI/RGO through the microemulsion solvothermal method (reproduced from Ahuja *et al.*, 2018 (ref. 301) (Open Access)) and (b) PANi/CNT/TiO_2 through the hydrothermal and sol–gel methods (reproduced with permission from Hung *et al.*, 2017 (ref. 302)).

5.3. Other methods

Various other methods reported for synthesizing PANI-based ternary composites include Pickering emulsion, solvothermal, hydrothermal, microemulsion-solvothermal, sol–gel, electrochemical polycondensation with dip-coating, co-precipitation with heating, and chemical reduction. Zhang *et al.*[300] prepared

 © 2026 The Author(s). Published by the Royal Society of Chemistry

Open Access Article. Published on 12 February 2026. Downloaded on 3/23/2026 6:55:17 AM.
This article is licensed under a Creative Commons Attribution 3.0 Unported Licence.

PANI–Fe_3O_4@ZnO *via* the Pickering emulsion route, which was found to be efficient for the degradation of MB dye. In another study, 98% of MB dye was removed using a NiO@PANI/rGO composite synthesized *via* the microemulsion solvothermal method. In this process, pre-synthesized PANI/GO served as the matrix, providing a surface for the growth of NiO microspheres *via* the microemulsion route, as shown in Fig. 5a.[301] Hung *et al.*[302] synthesized PANI/CNT/TiO_2 through two methods, *i.e.*, sol–gel and hydrothermal processes, for the removal of diethyl phthalate, as illustrated in Fig. 5b. Zhou *et al.*[303] reported electrochemical polycondensation by a dip coating method for the synthesis of g-C_3N_4 and PANI-co-modified TiO_2 nanotube arrays for efficiently removing tetrabromobisphenol A. This method provides better control over the thickness of PANI on surfaces and also ensures the adhesion of the polymer layer.

6. Mechanistic insights of PANI-based ternary photocatalysts

Typically, when a crystalline semiconductor photocatalyst (*e.g.* ZnO, TiO_2, and Fe_2O_3) is exposed to a photon energy ($h\nu$) higher than that of its E_g, it leads to the separation of charge carriers,[304] as depicted in Fig. 6a. Under light irradiation ($h\nu > E_g$), the electrons (e^-) in the VB (having related potential referred to as E_{vb}) of the semiconductor get excited to the CB (having related potential referred to as E_{cb}), leaving behind positively charged h^+. These photogenerated e^-/h^+ pairs then participate in redox reactions within their respective bands, generating ROS such as $^{\bullet}OH$ and $^{\bullet}O_2^-$.[12,305] Moreover, due to the electrophilic nature possessed by these radicals,[306] they are endowed with a powerful oxidizing ability ($^{\bullet}OH$: 2.73 eV *vs.* NHE, and $^{\bullet}O_2^-$: −0.33 eV *vs.* NHE)[305] and can account for the degradation of almost all electron-rich compounds (*e.g.* carbamazepine and bisphenol A)[307] to CO_2 and H_2O, thereby ensuring complete mineralization.[17,18] However, single-material photocatalysts come with their inherent limitations. For example, ZnO and TiO_2 suffer from a wide E_g that confines its application within a harmful UV range, while Fe_2O_3 experiences rapid e^-/h^+ recombination, which, in turn, hampers photocatalytic activity.[17,252,300,308] Notably, a visible-light-driven single-material photocatalyst (E_g < 3 eV) cannot generate $^{\bullet}OH$ and $^{\bullet}O_2^-$ radicals simultaneously because the disparity between their redox potential is 3.06 eV, as illustrated in Fig. 6b and listed in Table S1. Hence, researchers have explored various types of binary and ternary heterojunction materials to overcome the abovementioned challenges.

6.1. Types of heterojunctions

A single material can be modified by fabricating a heterojunction photocatalyst involving the coupling of semiconductors with dissimilar electronic band structures. This, in turn, complements each other and enhances the overall photocatalytic activity of the materials.[309] To date, heterojunctions have been reported comprising conventional types (types I, II, and III), p–n, Z-scheme and S-scheme heterojunctions.[12,14,18,310–312] Depending on the band alignment, the composite material establishes a new charge carrier transfer passage across the heterointerface, affirming the type of heterojunction formed. For instance, the type I heterojunction is formed when the energy bands (CB and VB) of photocatalyst-A are fully enclosed within that of photocatalyst-B,[313] as shown in Fig. 7a. This straddling gap results in poor charge carrier separation and reduced redox potential due to the accumulation of e^- and h^+ on the CB and VB of the photocatalyst B, respectively.[314]

On the other hand, the type II heterostructure is formed when the energy band configuration presents a staggered gap (Fig. 7b).[4,310] In this configuration, the VB of the photocatalyst A and the CB of the photocatalyst B are located within the E_g of the B and A photocatalysts, respectively. Although this arrangement suppresses charge recombination by directing electrons to the B photocatalyst and holes to the A photocatalyst, it lowers the

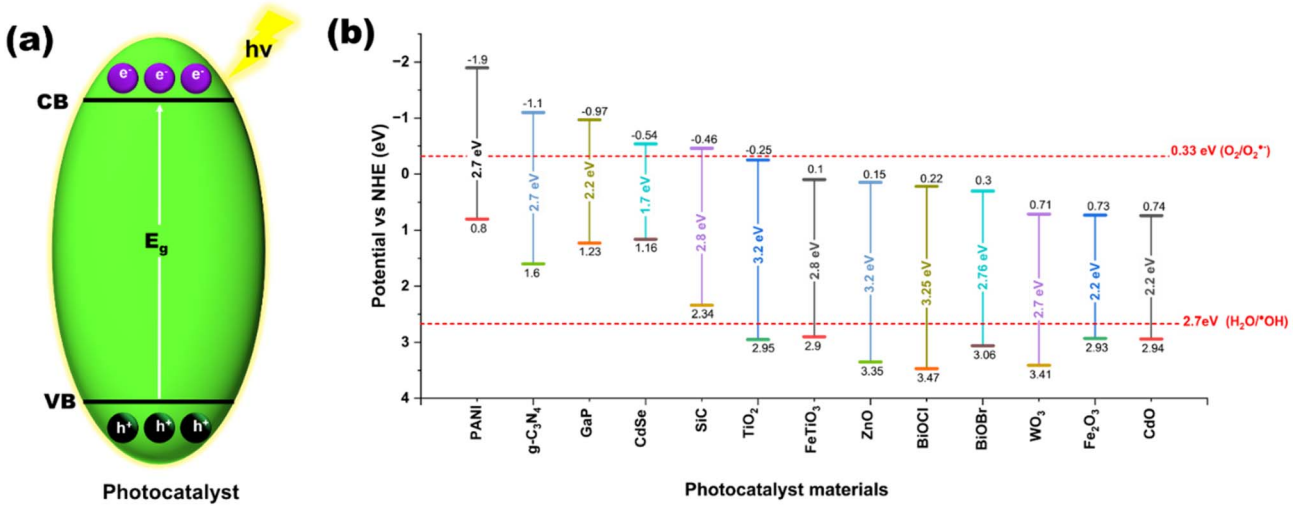

Fig. 6 (a) Electronic band structure of a semiconductor. (b) Position of the valence band (VB) and conduction band (CB) of various visible-light-driven photocatalysts with respect to the redox potential of $^{\bullet}OH$ and $^{\bullet}O_2^-$ (source: Table S1).

Open Access Article. Published on 12 February 2026. Downloaded on 3/23/2026 6:55:17 AM.
This article is licensed under a Creative Commons Attribution 3.0 Unported Licence.

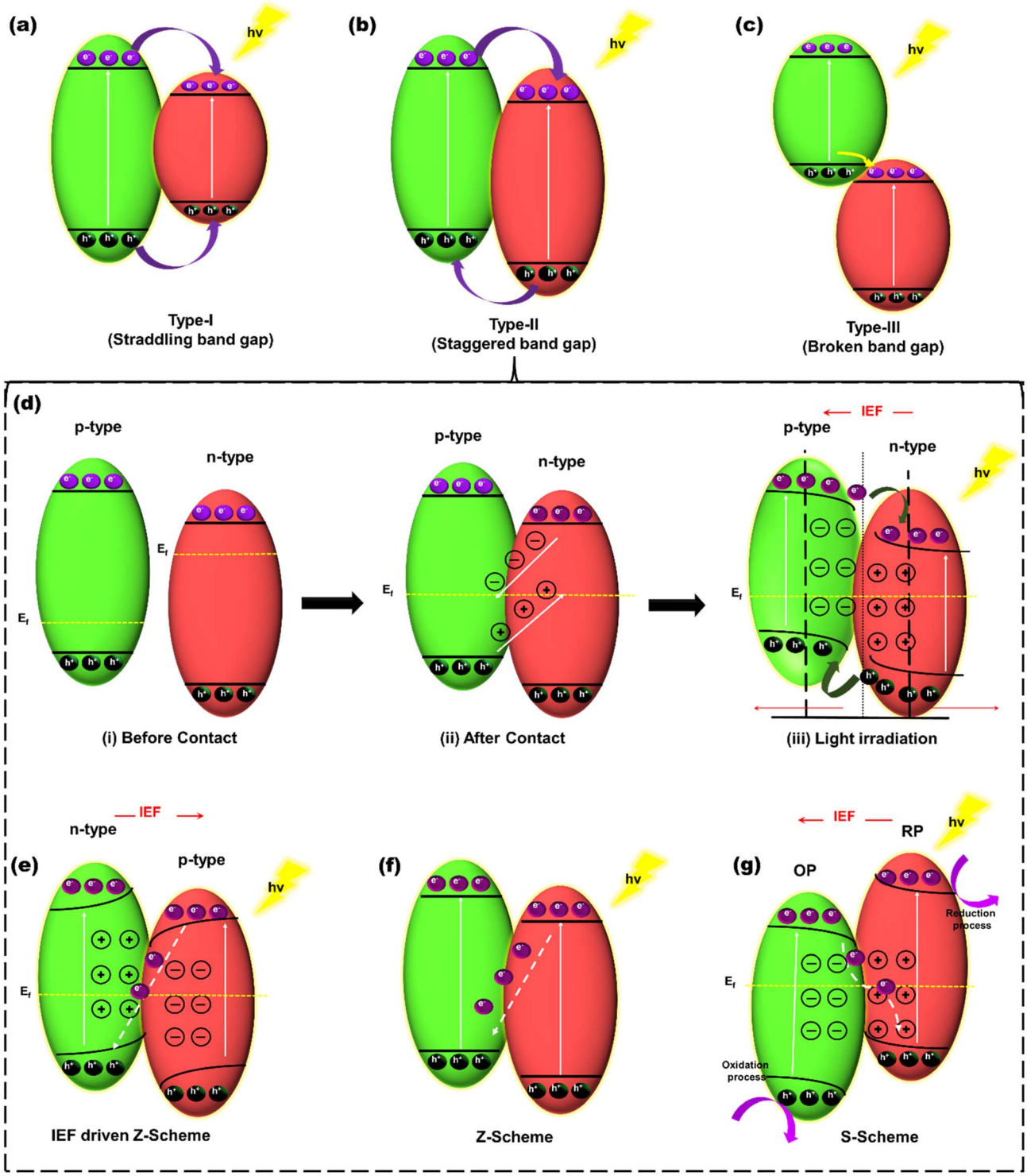

Fig. 7 Various mechanisms based on the type of heterojunctions: (a) type I, (b) type II, and (c) type III. Subtypes of the staggered band gaps: (d) p–n heterojunction: (i) before contact, (ii) after contact, (iii) and under light irradiation. (e) IEF-driven Z-scheme, (f) Z-scheme, and (g) S-scheme.

overall redox potential, as these charge carriers accumulate in bands with a weaker redox potential.[17,315] The conventional type of heterojunction is type III, also referred to as broken gap heterojunction (Fig. 7c).[314] This type of band alignment hampers the migration of charge carriers across the interface, resulting in their prompt recombination.[313] Therefore, the researchers have considered it to be the least favorable for the photocatalytic degradation of organic compounds. Based on the above discussion, the type II heterojunction photocatalyst illustrates attributes that are better than type I and type III heterostructures. However, it confronts challenges such as charge transfer barriers due to the electrostatic force at the

 © 2026 The Author(s). Published by the Royal Society of Chemistry

Open Access Article. Published on 12 February 2026. Downloaded on 3/23/2026 6:55:17 AM. This article is licensed under a Creative Commons Attribution 3.0 Unported Licence.

heterointerface and reduced overall redox potential. Researchers sought other possibilities within the staggered E_g configuration to address the limitations of conventional type II heterojunction.[17,18] Following this, the p–n heterojunction has emerged as a promising alternative, laying the foundation for the development of Z- and S-scheme heterojunctions, also identified as sub-types of type II heterojunctions.

For a p-type photocatalyst, the Fermi level (E_f) is positioned near the VB, whereas it is close to the CB for the n-type photocatalyst.[18] Fig. 7d(i) depict a couple of typical p- and n-photocatalysts (before contact), exhibiting the respective E_f positions, which are explicitly higher for n-type and lower for p-type photocatalysts. As soon as they come into contact, e^- flows from the n-photocatalyst type to the p-type photocatalyst until their E_f equalizes (Fig. 7d(ii)), causing their band to bend upward and downward, respectively.[316] The initial disparity in E_f drove e^-, thus inducing the internal electric field (IEF) oriented to the p-type photocatalyst. Upon irradiation, the migration of photogenerated e^-/h^+ pairs obeys the thermodynamics principles similar to that of conventional type II heterojunctions (Fig. 7d(iii)).[317] Moreover, the IEF offers an electrostatic effect to the p–n heterojunction, thereby regulating the charge transfer in a more efficient way[318] than that of conventional type II heterojunctions. Nevertheless, the reduced overall potential remains a challenge that may be addressed by the following heterojunction type.

The next alternative is the n–p heterojunction, as illustrated in Fig. 7e. Unlike the p–n heterojunction, the CB and VB position of the n-type photocatalyst is located at a higher energy side than the p-type photocatalyst. Up to their compounding stage, a similar mechanism would be followed as that in the p–n heterojunction but in reverse orientation. Furthermore, under the action of photon energy, the photogenerated e^-/h^+ was supposed to move as per the thermodynamics, but the band bending and IEF at the interface resist such migration. Another possibility is the migration of e^- and h^+ from the CB and VB of p-type photocatalysts to those of n-type photocatalysts. Such migration does enhance the overall redox potential but violates the basic thermodynamic principle. Thus, this route of e^-/h^+ is also not possible. However, if the arrangement of n–p heterojunction is carefully observed in Fig. 7e, there is one more possibility where e^- from the CB of p-type combines with leftover h^+ at the VB of the n-type photocatalyst due to their adjacency (Fig. 7e). Such pathway is supported by thermodynamics and is typically observed in the Z-scheme heterojunction.[319] In fact, not only the recombination of charge carriers reduced, but also the overall redox potential to degrade organic contaminants was enhanced. For instance, Nayak *et al.*[320] reported a case where a Z-scheme mechanism was established *via* a p–n heterojunction in the MoS_2/NiFe LDH nanocomposite.[320] Of note, there may not be IEF-induced charge carrier regulation across the Z-scheme heterointerface (Fig. 7f), as documented by Parida *et al.*[321] and Rawat *et al.*[17]

The observed demerits in type II and Z-scheme heterojunctions spurred the quest for further advancements.[322] Consequently, the S-scheme heterojunction was introduced by coupling a reduction photocatalyst (RP) and an oxidation photocatalyst (OP). In the S-scheme heterojunction, the VB and CB of RP have higher energy levels than those of OP. Moreover, the E_f value is higher for RP, demonstrating a lower value of work function than OP.[18] When RP and OP contact, the charge carriers are redistributed. As shown in Fig. 7g, e^- moves from the RP and accumulates near the OP to attain the equilibrium, which relocates respective E_f to the same energy level, thereby causing band bending and generation of IEF directed towards the OP.[12] Under light exposure, unlike the Z-scheme, the photoinduced e^- and h^+ are simultaneously generated by the RP and OP.[323] Subsequently, the weaker e^- and h^+ in the CB of OP and the VB of RP, respectively, recombine at the interface. The e^- in the CB of RP and the h^+ in the VB of OP possess strong redox potential, and their recombination is ceased due to the upward CB bending. Although the limitations are subsequently addressed, the absorption of visible light by the S-scheme photocatalyst needs to be rectified. As in numerous cases, the S-scheme heterostructure was driven by the UV light. According to the literature, researchers have addressed this issue by incorporating a third co-catalyst, forming a ternary heterojunction capable of absorbing visible light.[292,300,303,308,312,324–331]

6.2. PANI-based ternary heterojunctions

PANI displays a semiconductor-like activity due to π electron delocalization along its polymer backbone.[327] PANI does not hold the regular atomic arrangement characteristic of crystalline semiconductors. However, based on the molecular orbital theory, its electronic structure can be perceived as analogous to that of inorganic semiconductors.[332] The HOMO and LUMO of PANI represent the VB and CB, respectively. Furthermore, the E_g between these molecular orbitals dictates the threshold energy required to stimulate the electron from the HOMO to the LUMO.[333] Several studies have reported a narrow E_g value of approximately 2.7 eV for PANI, which highlights its potential for visible-light-driven photoactivation.[300,308,329,330] Moreover, it demonstrates a large surface area and excellent electron-donating and hole-accepting properties, and stabilizes the photocatalyst.[300,308,312,324–326,330] Thus, PANI can function as a photosensitizer, charge mediator (bridge), and protective layer, making it an appropriate contender for ternary composites or heterojunctions.

These statements reasonably aligned with the inferences drawn by Tanwar *et al.*[329] In their study, they prepared a PANI/Fe^0/BiOCl (BPF) composite and demonstrated that PANI could act as a modifier, photosensitizer and stabilizer (as a photocorrosion inhibitor) in BPF (Fig. 8a). This is also quite evident from the BPF optical properties, indicating reduced E_g and PL spectra intensity. Moreover, charge carrier transfer occurred in a way that the photoexcited e^- migrated from the LUMO of PANI to the CB of BiOCl, just as the photogenerated h^+ transferred to the HOMO of PANI from the VB of BiOCl.[329] Similarly, Zhang *et al.*[300] exploited the narrow E_g of PANI to make ZnO-shelled PANI–Fe_3O_4 (PANI–Fe_3O_4@ZnO) active in the visible light region. Under irradiation, PANI absorbed visible light and induced π → polaron and polaron → π* transitions, resulting in the transfer of the excited state e^- to the π* orbital (LUMO),

Open Access Article. Published on 12 February 2026. Downloaded on 3/23/2026 6:55:17 AM.
This article is licensed under a Creative Commons Attribution 3.0 Unported Licence.

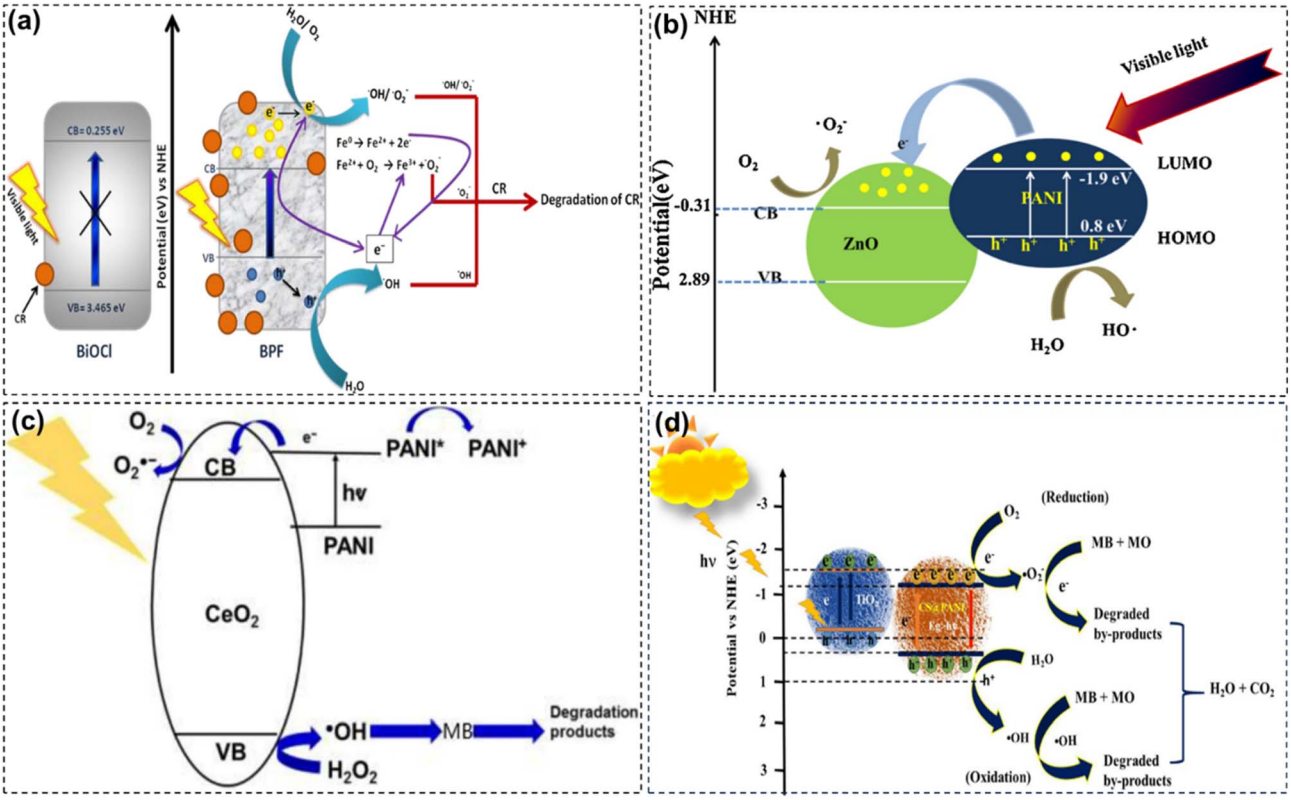

Fig. 8 PANI employed primarily as a photosensitizer in ternary composites: (a) PANI/Fe^0/BiOCl (reproduced with permission from Tanwar *et al.*, 2017 (ref. 329)), (b) PANI-Fe_3O_4@ZnO (reproduced with permission from Zhang *et al.*, 2016 (ref. 300)), (c) PS/PANI/CeO_2 (reproduced with permission from Chen *et al.*, 2022 (ref. 328)), and (d) TiO_2@CS-PANI (reproduced from Palliyalil *et al.*, 2022 (ref. 308) (Open Access)).

reasonably matching with the d-orbital (CB) of TiO_2, thereby causing the synergistic effect (Fig. 8b). This advanced the photogenerated e^- from the LUMO of PANI to the CB of ZnO. As a result, $^{\bullet}OH$ and $^{\bullet}O_2^-$ radicals were produced, which degraded the organic dyes.[300] Moreover, PANI served as a photosensitizer to PS/CeO_2, enhancing the overall E_g of PS/PANI/CeO_2 to 2.93 eV from 3.19 eV (Fig. 8c).[328] Similarly, in another ternary composite, TiO_2@CS–PANI exhibited a reduced E_g value of 2.98 eV compared to the E_g value of 3.2 eV of TiO_2. Thus, it is transformed into a significant visible light-driven ternary composite (TiO_2@CS–PANI) (Fig. 8d) degrading 92.3% and 89.5% of toxic MB and MO dye molecules, respectively.[308] Notably, PANI as a sensitizer is significant in incorporating it with broad E_g (>3 eV) semiconductors, including BiOCl, ZnO, TiO_2, and CeO_2, as mentioned above. Several studies have also established the role of PANI as a charge mediator, functioning as an e^- bridge between co-photocatalysts in the ternary composite, thereby elevating the charge carrier conveyance. For instance, Li *et al.*[330] synthesized a ternary composite (g-C_3N_4-PANI-MoS_2), where PANI served as a conductive bridge between g-C_3N_4 and MoS_2. Reportedly, the composite exhibited the highest photocurrent density, confirming the formation of a photo-induced charge transfer pathway. Electrochemical impedance spectroscopy (EIS) further validated this result, highlighting the strong interfacial connection and promoting efficient e^- migration.[330] Chopan and Chishti demonstrated the rapid migration of the photogenerated e^- from the CB of α-MnO_2 to the VB of g-C_3N_4 *via* the PANI bridge (Fig. 9a), thereby accelerating charge transfer.[324] In another study,[312] a dual p–n heterojunction was established to enable the degradation of tetracycline. Incorporating 10% PANI into MIL-88B@COF-200 enhanced the charge carrier mobility and extended visible light absorption. As illustrated in Fig. 9b, the e^- from LUMO of the PANI (p-type photocatalyst) is transferred to the corresponding CB of COF-200 (n-type photocatalyst) and MIL-88B (n-type photocatalyst). Moreover, the h^+ from the HOMO of PANI migrates to the VB of the respective n-type photocatalysts, which, in turn, forms a dual p–n heterojunction. Notably, the internal electric field (IEF) further facilitated charge carrier transport through PANI, leading to enhanced photocatalytic activity.[312]

Besides acting as a photosensitizer and a charge carrier mediator, PANI can serve as a protective layer in the ternary composite, inhibiting photo-corrosion and stabilizing the photocatalyst, promoting interfacial charge dynamics. For illustration, Mousli *et al.*[331] reported a core–shell TiO_2-DPA-PANI nanocomposite (Fig. 10a), where PANI encapsulates the TiO_2 core, while DPA acts as a binding agent between PANI and TiO_2. Moreover, the ternary composite exhibited the highest apparent degradation rate constant, explicitly demonstrating PANI's role in enhancing the photocatalytic activity and protecting TiO_2 under UV light.[331] In another study, PANI was used to inhibit photocorrosion, thereby improving the stability of the composite. For instance, Lin *et al.*[292] (Fig. 10b) and Yu *et al.*[325]

 © 2026 The Author(s). Published by the Royal Society of Chemistry

Open Access Article. Published on 12 February 2026. Downloaded on 3/23/2026 6:55:17 AM.
This article is licensed under a Creative Commons Attribution 3.0 Unported Licence.

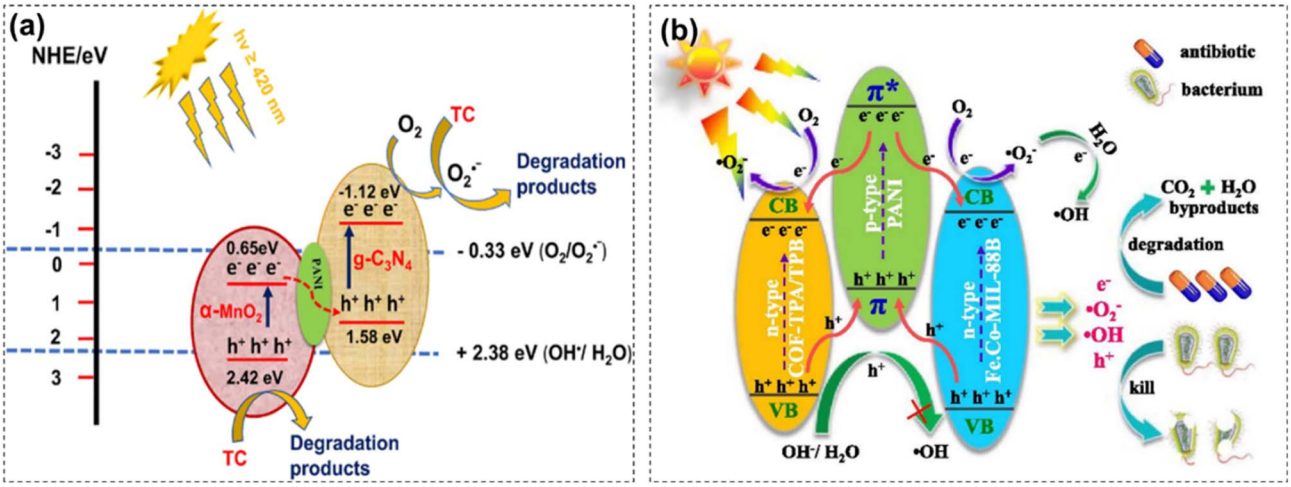

Fig. 9 PANI employed primarily as a charge carrier bridge (mediator) in ternary composites: (a) g-C_3N_4/PANI/α-MnO_2 (reproduced with permission from Chopan and Chishti, 2023 (ref. 324)) and (b) MIL-88B@COF-200@10%PANI (reproduced with permission from Lv *et al.*, 2021 (ref. 312)).

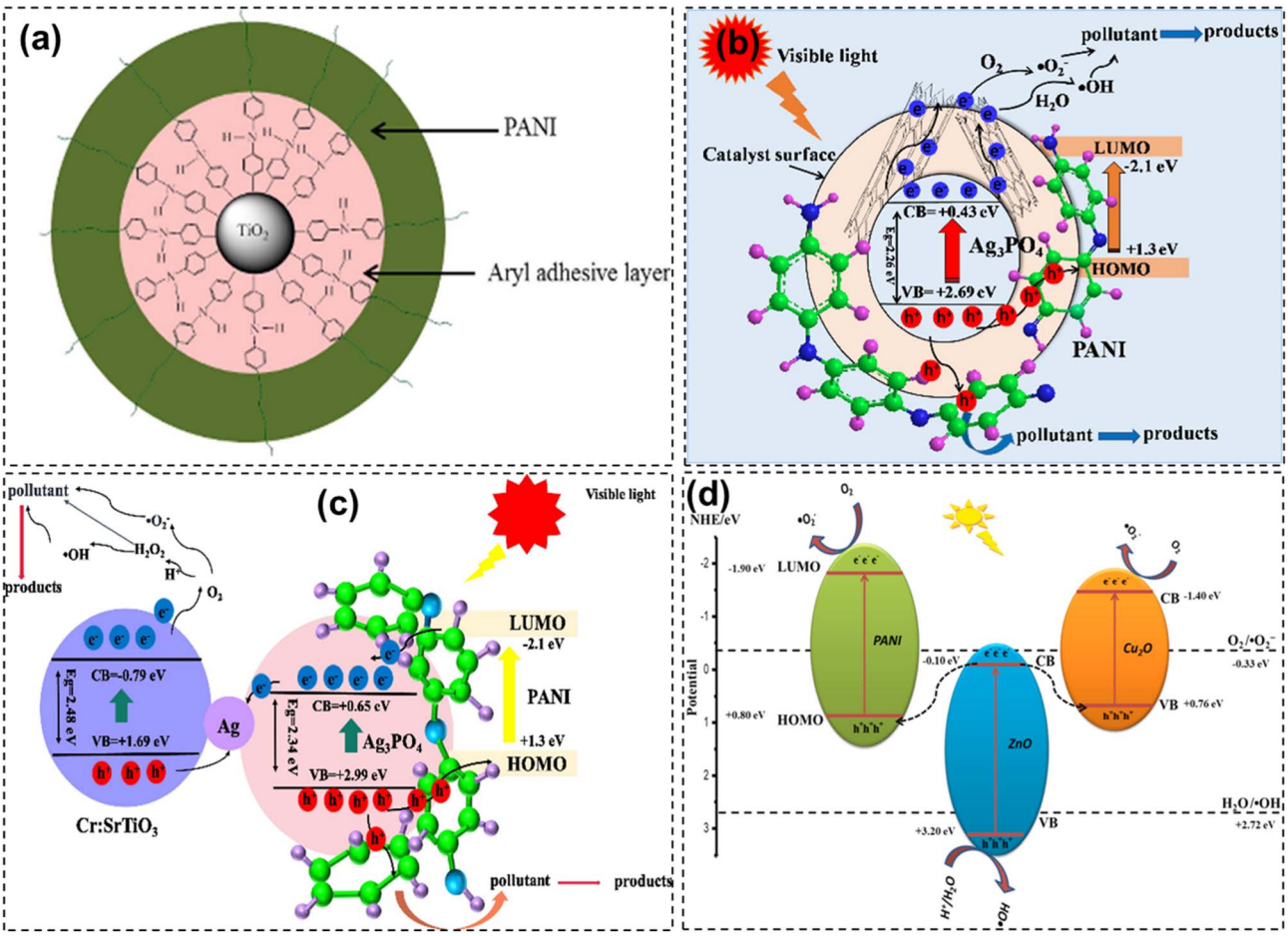

Fig. 10 PANI employed as a stabilizer in ternary composites: (a) core–shell TiO_2-DPA-PANI nanocomposites (reproduced with permission from Mousli *et al.*, 2019 (ref. 331)), (b) Ag_3PO_4@MWCNTs@PANI (reproduced with permission from Lin *et al.*, 2019 (ref. 292)), (c) Ag_3PO_4/PANI/Cr:$SrTiO_3$ (reproduced with permission from Yu *et al.*, 2020 (ref. 325)), and (d) Cu_2O/ZnO-PANI (reproduced with permission from Mohammed *et al.*, 2021 (ref. 326)).

Open Access Article. Published on 12 February 2026. Downloaded on 3/23/2026 6:55:17 AM. This article is licensed under a Creative Commons Attribution 3.0 Unported Licence.

(Fig. 10c) incorporated PANI to avoid the photocorrosion of Ag_3PO_4 in the composite of Ag_3PO_4@MWCNTs@PANI and Ag_3PO_4/PANI/Cr:$SrTiO_3$, respectively. In addition, their respective mechanisms are illustrated in Fig. 10b (ref. 292) and 10c.[325] Similarly, the photocorrosion of Cu_2O was effectively prevented using PANI, thus forming a stable dual Z-scheme ternary photocatalyst heterojunction, as depicted in Fig. 10d.[326]

7. PANI-based ternary composites for the degradation of organic pollutants

7.1. Dyes

Dyes are typically known for imparting colour by forming physical or chemical bonds with the substrate to which they are applied. In this context, a diverse range of dyes originate from various sectors, including textiles, pharmaceuticals, leather industry, food industry, household products, and wastewater treatment facilities, ultimately impacting freshwater sources.[15,334,335] Dyes are harmful pollutants that do not break down easily and are also toxic. Their presence in natural water sources causes serious health and environmental issues.[336,337] Their release causes eutrophication, deteriorates the freshwater quality and could cause skin irritation, allergy, dermatitis, and organ damage including cancer.[338–341] This highlights the need for the removal of dyes from the water sources. Dyes can be classified into anionic and cationic dyes based on their molecular charges.[20] Anionic dyes include MO, alizarin yellow, and Eriochrome black T (EBT), whereas cationic dyes include MB, RhB, and crystal violet.[342,343]

According to Dhanda *et al.*[344] PANI@Er-doped ZnO has approximately 89% removal efficiency for MB dye at pH 7 in 90 min. The degradation efficiency is influenced by factors such as the direction of charge carrier migration, reduced recombination rate of photo-generated e^-/h^+ pairs, and their effective separation within the synthesized nanocomposite. Additionally, Pandiselvi *et al.*[345] reported a 90% reduction of MB by the novel PANI-based ternary hybrid photocatalyst g-C_3N_4/PANI/ZnO in 80 min. This hybrid photocatalyst provided a low recombination rate of e^-/h^+ pairs, and PANI enhanced the visible photocatalytic performance by improving the visible light absorption intensity. Notably, PANI also acted as an electron mediator, as reported by Lai *et al.* 2025 in a novel g-C_3N_4/V_2O_5/PANI ternary composite, following type II pathway for 99% degradation of MB under the optimal conditions of a catalyst dose of 1.5 g L^{-1} and an initial concentration of 5 mg L^{-1} at pH 7 in 120 min, with $^{\bullet}OH$ and $^{\bullet}O_2^-$ as major ROS involved in degradation.[346] Reportedly, PANI-based ternary photocatalysts are highly efficient in the degradation of MB dye.[252,270,300,301,308,328,347–352] Asghar Jamal *et al.*[352] reported that the removal efficiency of 10 mg of GO/Fe_3O_4/PANI for 10 ppm of RhB dye is more than 92% in 60 min under natural sunlight. The GO/Fe_3O_4/PANI photocatalyst is reported to be efficient in the removal of RhB due to its porous surface that allows better interaction with ROS, utilization of a maximum portion of sunlight, and also a lower dose of the photocatalyst. The authors have mentioned that the removal of RhB was mainly triggered by $^{\bullet}O_2^-$. Bu and Chen[183] investigated the degradation of RhB by the PANI/Ag/Ag_3PO_4 ternary composite and observed more than 95% removal of the dye. This enhancement can be attributed to the formation of a heterojunction electric field between PANI and $AgNO_3$, which improved the separation efficiency of photogenerated e^-/h^+ pairs and facilitated the transfer of photogenerated holes from Ag_3PO_4 to PANI, thereby inhibiting the self-oxidation of Ag_3PO_4. Furthermore, numerous studies have been documented concerning the effective photodegradation of RhB using the developed PANI-based ternary catalyst.[189,271,347,353–356] In another work, a novel photocatalyst TiO_2/PANI/GO degraded Thymol blue and Rose Bengal to nearly 85% and 99%, respectively, in 180 min.[357] Similarly, Cui *et al.*[217] reported 99.7% degradation of the Congo red dye by a TPU/TiO_2/PANI membrane within 30 min. In both the aforementioned studies, $^{\bullet}O_2^-$ and $^{\bullet}OH$ radicals are involved in the photocatalytic degradation of the Congo red dye.[251,357] Reportedly, the PANI/GO/MoO_3 (PGMO) nanocomposite was employed for the degradation of MO, showing 98.9% under optimum conditions of 0.2 g L^{-1} catalyst dose for the 20 mg L^{-1} of initial concentration at pH 6.8 in 120 min of irradiation. A scavenging experiment was conducted for the identification of specific radical species playing a role in the charge transfer mechanism. The authors mentioned that methanol, iso propyl alcohol (IPA), and benzoquinone (BQ) affected the efficiency, indicating the participation of h^+, $^{\bullet}OH$, and $^{\bullet}O_2^-$ in the charge transfer pathway. The results conclude the occurrence of the Z-scheme pathway between the ternary composites, where PANI is acting as the photosensitizer with a band gap of 2.7 eV.[69] Mousli *et al.*[331] prepared TiO_2-DPA-PANI, which degraded the MO dye with an efficiency of 99.5% under UV irradiation in 20 min, ascribed to the quantity of PANI deposited on the surface of TiO_2, where PANI acts as the e^- donor and h^+ acceptor, facilitating the generation of $^{\bullet}O_2^-$ and $^{\bullet}OH$ radicals. Similarly, Mitra *et al.*[311] mentioned the degradation of MO and Rose Bengal with efficiencies of 92.5% and 98%, respectively, under visible light irradiation in 150 min, attributed to the introduction of PANI in Al-doped ZnO. Zhao *et al.*[358] utilized TiO_2/PANI/GO to achieve 98.2% MO degradation in 90 min. This enhanced performance was attributed to the role of PANI and GO in facilitating the transfer of h^+ from the VB of TiO_2 to the HOMO of PANI, as evidenced by the reduced fluorescence intensity, thereby suppressing e^-/h^+ recombination. Moreover, Turkten *et al.* 2025 studied the removal of reactive blue-198 dye over the synthesized novel p–n–p-type PANI-TiO_2-CuO composite, which showed 90.4% photocatalytic efficiency within 60 min under an optimized catalyst dose of 0.25 g L^{-1} and an initial concentration of 10 mg L^{-1}.[357] Interestingly, the Z-scheme pathway was followed in the Cu_2O/ZnO-PANI (CZP) composite, degrading 100% of CR in 30 min of irradiation at an optimum dose of 1 g L^{-1} and an initial concentration of 30 mg L^{-1} at pH 6, attributed to the role of PANI as a photocorrosion inhibitor. The authors have analysed the charge transfer mechanism through scavenging studies, which elucidated that ammonium oxalate and benzoquinone lead to a significant decrease in degradation efficiency, revealing h^+ and $^{\bullet}O_2^-$ as primary active species.[326] Hence, the photocatalytic removal of these pollutants is directly governed by the

 © 2026 The Author(s). Published by the Royal Society of Chemistry

Open Access Article. Published on 12 February 2026. Downloaded on 3/23/2026 6:55:17 AM.
This article is licensed under a Creative Commons Attribution 3.0 Unported Licence.

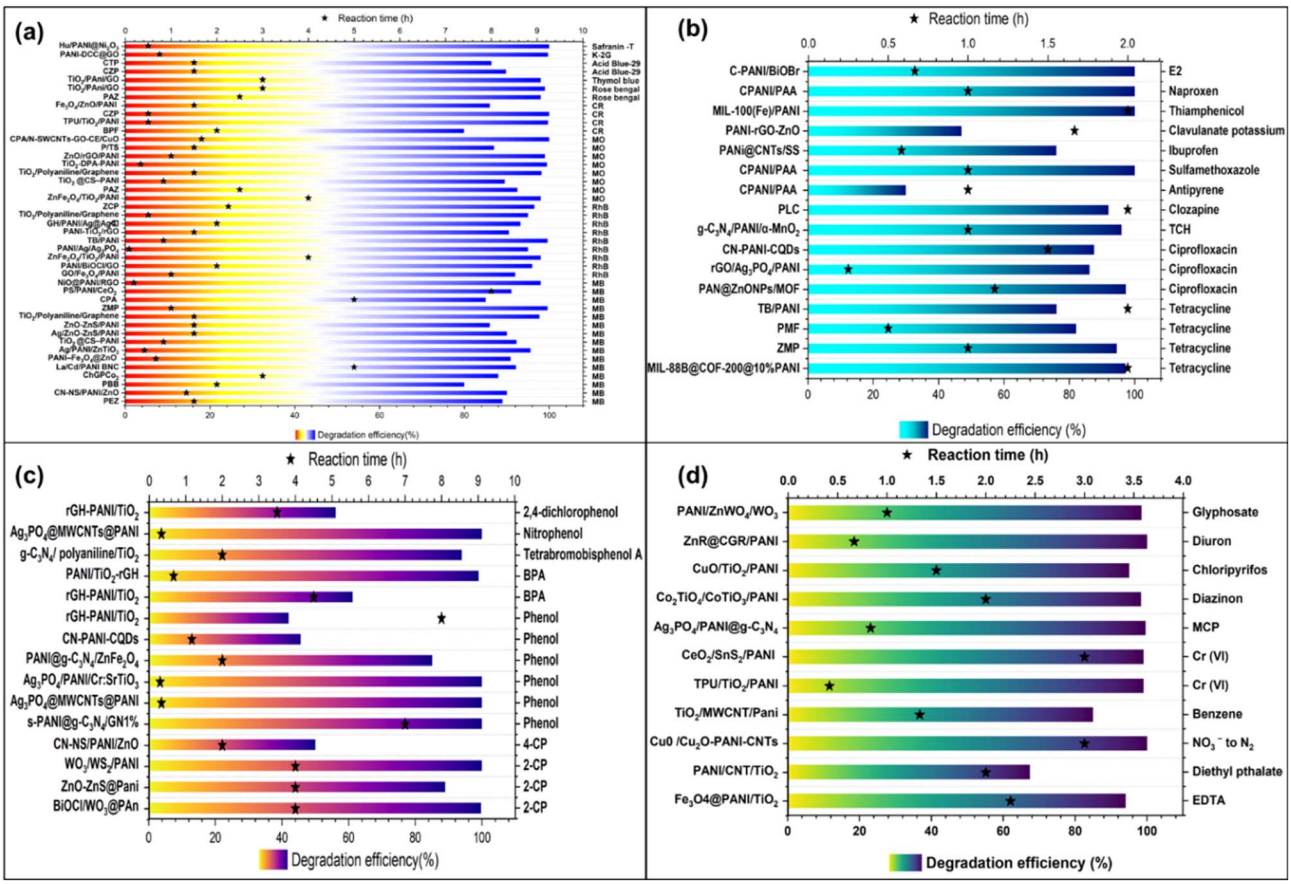

Fig. 11 Application of the PANI-based ternary composite for the photodegradation of (a) dyes (source: Table S2), (b) pharmaceutically active compounds (source: Table S3), (c) phenolic compounds (source: Table S4), and (d) others (source: Table S5).

generated reactive oxygen species (ROS), participating in the degradation mechanism. Fig. 11a presents the PANI-based ternary photocatalysts that achieved significant dye degradation efficiencies within specific reaction times. The detailed performance data of various photocatalysts for dye removal from wastewater are summarized in Table S2.

7.2. Pharmaceutically active compounds (PhACs)

Pharmaceutically active compounds (PhACs) are commonly used in the treatment and prevention of infections and diseases in humans and animals.[359,360] It includes a wide variety of antibiotics, antimicrobials, antidepressants, painkillers, anti-inflammatory agents, and hormones.[20,361] The extensive use of pharmaceuticals, the rising prevalence of chronic diseases, and the continuous development of new drugs have led to the generation of large volumes of pharmaceutical waste.[361,362] PhACs including tetracycline,[363] tetracycline hydrochloride,[324] ciprofloxacin,[364] 17β-estradiol,[295] clozapine,[365] antipyrine,[366] ibuprofen, sulfamethoxazole,[366] and naproxen[366] have been successfully removed by PANI-based ternary photocatalysts. The degradation of tetracycline using PANI/$CoFe_2O_4$/WO_3 (PCFW) synthesized by the microwave-assisted ionic liquid method has been previously reported.[363] Barik *et al.*[363] have mentioned more than 99% degradation efficiency of PCFW after a reaction time of 50 min. This enhancement is attributed to the increased surface area of the PCFW ternary heterojunction resulting from the addition of PANI, which promotes nanostructure aggregation and improves porosity distribution within the metal oxide framework. Similarly, Lv *et al.*[312] reported the synthesis of MIL-88B@COF-200@10%PANI that removed tetracycline with 97.2% efficiency within 120 min, attributed to the introduction of PANI holding a π–π conjugated structure, which acted as a charge transporter fostering the charge carrier movement, increasing absorption in the visible light region, the formation of double p–n junctions and the inhibition of photogenerated e^-/h^+ recombination. In a study, about 96% removal efficiency of tetracycline hydrochloride (TCH) is achieved in 60 min by the g-C_3N_4/PANI/α-MnO_2 composite under visible light irradiation.[324] The large surface area of the photocatalyst, along with the quenching of photoluminescence, promotes the effective separation of electron–hole (e^-/h^+) pairs and reduces their recombination rate along with the large amount of $^{\bullet}O_2^-$ and $^{\bullet}OH$, e^-, and h^+, accounting for the observed high-efficiency removal of TCH. Wang *et al.*[364] synthesized rGO/Ag_3PO_4/PANI for preventing the photo-corrosion of Ag_3PO_4, where PANI served as a h^+ transporter, whereas rGO was used as an electron transporter in the degradation of ciprofloxacin, achieving an efficiency of 86.2% within 15 min. Kumar *et al.*[365] reported 94.2% degradation of clozapine utilizing the ternary PANI/$LaFeO_3$/$CoFe_2O_4$ heterojunction in 120 min at an optimized

Open Access Article. Published on 12 February 2026. Downloaded on 3/23/2026 6:55:17 AM. This article is licensed under a Creative Commons Attribution 3.0 Unported Licence.

doze of 0.3 g L^{-1}. The high negative potential of the LUMO of PANI facilitates charge transfer to molecular oxygen, leading to ROS generation, heterojunction formation, visible-light-active band formation, and a comparatively lower charge carrier recombination rate. Qing *et al.*[295] reported the 100% removal of 17β-estradiol (E2) using a C-PANI/BiOBr S-scheme heterojunction in 40 min. This can be attributed to the S-scheme heterojunction, adsorption capacity of C-PANI because of the π–π stacking interaction between the aromatic rings of E2 and PANI and the primarily exposed crystal plane that promoted enhanced separation of photogenerated charge carriers. In 2025, Ren *et al.* have prepared novel $BiVO_4$/g-C_3N_4/PANI, which displayed 91% removal efficiency for enrofloxacin under an optimal catalyst dose of 1 g L^{-1} and an initial concentration of 10 mg L^{-1}, attributed to the Z-scheme charge transfer pathway and $^{\bullet}O_2^-$ and $^{\bullet}OH$ radicals validated by electron spin resonance (ESR) spectroscopy.[367] These studies highlighted that the formation of heterojunctions facilitated efficient separation of charges, leading to a lower recombination rate and the generation of more ROS. The addition of PANI increases the surface area and porosity of the composite, which provides more active sites for photodegradation. In addition, the high negative potential of the LUMO of PANI facilitates the transfer of e^- to molecular oxygen. Fig. 11b displays the efficient degradation of PhACs by PANI-based ternary composites, while Table S3 summarizes the performance of various photocatalysts for PhAC removal from wastewater.

7.3. Phenolic compounds

Phenolic compounds are characterized by one or more hydroxyl groups directly bonded to an aromatic hydrocarbon group. R. Kumar *et al.*[368] prepared BiOCl/WO_3@PANI as an efficient photocatalyst degrading 99.7% of 2-chlorophenol under the optimum conditions in 240 min. This can be attributed to the addition of PANI, which enhanced visible light absorption and suppressed charge recombination, with $^{\bullet}O_2^-$ radicals actively contributing to the degradation. In another study, ZnO/ZnS@PANI degraded 89% of 2-chlorophenol within 240 min. This was attributed to PANI's ability to absorb a broad range of visible light and enhance e^-/h^+ separation.[369] Phenol was completely degraded (100%) under UV irradiation using an s-PANI@g-C_3N_4/GO composite within 7 h, which can be attributed to its smaller grain size and enhanced sp^2 network. The study concluded that sulfonation significantly improved phenol degradation, further enhanced by the optimum inclusion of GO.[370] In another study, PANI@g-C_3N_4/$ZnFe_2O_4$ degraded 85.1% in 120 min under visible light irradiation, which could be ascribed to a strong synergistic effect resulting from the electrostatic interaction between the components of the photocatalyst through physisorption, and efficient charge transfer.[371] A 100% degradation of phenol and nitrophenol was observed using Ag_3PO_4@MWCNTs@PANI after a reaction time of 20 min, which can be attributed to PANI acting as an efficient h^+ transporter, reducing the recombination rate of charge carriers and regulating the Ag_3PO_4 crystal size.[292] The PANI-based ternary composites demonstrated effective degradation of phenolic compounds, as shown in Fig. 11c. Table S4 presents the performance data for various photocatalysts utilized in the degradation of phenols from wastewater.

7.4. Others

PANI-based ternary photocatalytic materials have proven effective in the degradation of several other types of contaminants including pesticides, insecticides, volatile organic compounds (VOCs), and metals. In a study, Karamifar *et al.*[372] reported the degradation of benzene through TiO_2/MWCNT/Pani with an efficiency of 84.9% under optimum conditions in a reaction time of 80 min under visible light irradiation, which can be attributed to the role of $^{\bullet}OH$ and $^{\bullet}O_2^-$. Li *et al.*[373] reported the 94% degradation of ethylenediaminetetraacetic acid (EDTA) by a synthesized magnetically separable Fe_3O_4@PANI/TiO_2 photocatalyst under visible light irradiation in 135 min. The formation of the PANI-TiO_2 heterojunction enhanced the photoactivity by facilitating efficient charge separation and transfer, thus reducing the e^-/h^+ recombination. Balasubramanian *et al.*[374] synthesized Ag_3PO_4/PANI@g-C_3N_4, which degraded monocrotophos with a degradation efficiency of 99.6% under visible light in an irradiation time of 50 min, facilitated by $^{\bullet}OH$ and $^{\bullet}O_2^-$ radicals. PANI/CNT/TiO_2 was prepared by two different synthesis methods, the sol/gel method and the hydrothermal method, achieving 59% and 67.4% degradation of diethyl phthalate.[302] The PANI-based ternary composites demonstrated notable degradation efficiencies for various organic pollutants within the specified reaction time, as illustrated in Fig. 11d. Table S5 presents the performance data for various photocatalysts utilized in the removal of diverse compounds from wastewater.

Although the conventional factors influencing photocatalytic degradation were discussed in this section, other critical parameters such as the physicochemical properties of the target pollutants, interference from coexisting substances, and the characteristics of the water matrix also play a significant role in determining the overall effectiveness of photocatalytic processes. Thus, the subsequent section elucidates the other influencing parameters.

7.5. Role of multifunctional PANI in the proposed degradation pathways

The multifunctional role of PANI in the ternary system, as elucidated by mechanistic insights provided in Section 6.2, involves the generation of ROS, which govern the degradation products and pathways of organic pollutants. For instance, PANI was employed as a photosensitizer by Palliyalil *et al.* (2022) in a TiO_2@CS-PANI composite. Upon irradiation, PANI generated e^-/h^+ pairs, in which the photogenerated e^- was transferred to TiO_2, thereby averting the charge carrier recombination. The photogenerated h^+ in the VB oxidized H_2O molecules to produce $^{\bullet}OH$ radicals, while e^- in the CB reduced dissolved O_2 molecules to form $^{\bullet}O_2^-$ radicals. However, scavenging studies revealed that $^{\bullet}OH$ radicals played a predominant role in the photocatalytic degradation process. Consequently, the proposed degradation mechanism for both MB and MO dyes was initiated by $^{\bullet}OH$

 © 2026 The Author(s). Published by the Royal Society of Chemistry

Open Access Article. Published on 12 February 2026. Downloaded on 3/23/2026 6:55:17 AM. This article is licensed under a Creative Commons Attribution 3.0 Unported Licence.

radical attack. The degradation of MB led to the generation of intermediates with *m*/*z* values of 357, 324, 311, 74, 65, and 54, whereas in the case of MO, the transformation products had *m*/*z* values of 214, 174, 139, 74, and 65, and finally, transformed into CO_2, H_2O, and inorganic salts. The degradation pathways were estimated by liquid chromatography-mass spectrometry (LC-MS), in which the *m*/*z* values confirmed the sequential stages of chromophore cleavage, deethylation, aromatic ring opening, and mineralization of the above-mentioned dyes.[308] In another study, Basu *et al.* (2025) explored the same functionality of PANI in the PANI/GO/MoO_3 composite. Interestingly, the UV-DRS spectra showed a significant broadening of the visible light response range upon PANI incorporation, thereby enhancing the photocatalytic efficiency of MoO_3. Under irradiation, e^- was generated in the CB (GO and MoO_3) and in the LUMO of PANI, followed by the transfer of e^- from the CB of GO and MoO_3 into the HOMO of PANI. Simultaneously, the photogenerated h^+ at the HOMO of PANI enabled the oxidation of OH^- to $^{\bullet}OH$ radicals, while e^- reduced O_2 into $^{\bullet}O_2^-$ radicals. These ROS ($^{\bullet}O_2^-$, and $^{\bullet}OH$) and e^- mineralized MO, producing four intermediates with *m*/*z* values of 121, 136, 152, and 171, as confirmed by the gas chromatography-mass spectroscopy (GC-MS) technique.[353] Furthermore, Chopan and Chisti (2023) used PANI as a conductive bridge between α-MnO_2 and g-C_3N_4. As a result, the transmission of e^- from the CB of α-MnO_2 to the VB of g-C_3N_4 was accelerated across the heterointerface. Subsequently, $^{\bullet}O_2^-$, and $^{\bullet}OH$ radicals mineralized the tetracycline and produced several intermediate compounds with *m*/*z* of 462, 433, 413, 361, 362, 337, 297, 270, 258, 242, 213, 209, 175, 164, 134, 107, and 104, which were identified using High resolution-Mass Spectroscopy (HR-MS).[324] Similarly, Lv *et al.* (2021) reported plausible degradation pathways of tetracycline while introducing PANI into MIL-88B@COF-200@10%PANI, with a π–π conjugated structure acting as a bridge for charge transport. The specific arrangement of band positions was determined *via* UV-DRS and Mott–Schottky analyses, which leads to the generation of $^{\bullet}OH$, $^{\bullet}O_2^-$, h^+, and e^- as the main reactive species for tetracycline removal, proposing three pathways comprising nineteen intermediate products that ultimately mineralized to CO_2 and H_2O.[312]

Recently, the photocorrosion properties of PANI in ternary composites have also been exploited to improve the photostability of the composites. For instance, Wang *et al.* (2021) fabricated rGO/Ag_3PO_4/PANI for inhibiting the photocorrosion of Ag_3PO_4. In this system, photogenerated h^+ from the VB of Ag_3PO_4 migrated towards the PANI, which acted as the h^+ conductor. In parallel, e^- from the CB was transferred to rGO, which served as an e^- acceptor. This mechanism leads to the degradation of ciprofloxacin into disintegrated molecules, followed by three degradation pathways for the destruction of the piperazine ring of quinolone and the removal of fluorine, and major intermediate products were identified by HPLC-MS.[364] Moreover, Turkten *et al.* (2025) have used density functional theory (DFT) calculations to analyze the Fukui indices, identifying localized reactive sites responsible for organic pollutants. The high-value Fukui indices indicated atoms affected by $^{\bullet}OH$ attacks. The authors have also integrated the theoretical and experimental calculations for proposing the degradation mechanism of Reactive Blue 198 (RB-198) dye using a PANI-TiO_2-CuO ternary system and reported the breakdown of RB-198 into two fragments following two different pathways.[357] Collectively, these studies show the mechanistic role of PANI in the degradation pathways, enabling the identification of intermediates by LC-MS, GC-MS, HR-MS, HPLC-MS, and DFT, thereby strengthening the credibility of the proposed degradation pathways in ternary systems.

8. Other parameters influencing photocatalytic degradation using PANI-based ternary composites

8.1. Physicochemical properties of the target pollutants

For a given photocatalyst material (such as PANI-based ternary composites), the effectiveness of the photocatalytic degradation system is significantly influenced by the molecular structure, functional groups, and surface charge of the target pollutants, which collectively control the adsorption behaviour and interfacial reaction pathways.[347,375] PANI introduces a redox-active, pH-responsive polymeric component, making these systems particularly sensitive to the charge characteristics of pollutants.[376] As mentioned earlier, PANI contains alternating amine (–NH–) and imine (=N–) groups, whose protonation state varies with the pH.

In anionic pollutants such as MO and CR, which contain carboxylate and/or sulfonate groups, strong electrostatic attraction is typically observed when PANI is in its protonated state. For example, Zare *et al.*[377] reported a noticeable decrease in the degradation efficiency of CR over an Fe_3O_4/ZnO/PANI composite as the solution pH shifted from acidic to alkaline conditions. A similar pH-dependent trend was observed by Mousli *et al.*[331] during the photocatalytic degradation of MO using a TiO_2-DPA-PANI composite, underscoring the role of electrostatic interactions in enhancing adsorption and subsequent degradation under acidic conditions. However, cationic pollutants including MB and RhB tend to interact more favourably under conditions where PANI is partially deprotonated. Under such conditions, electrostatic repulsion is minimized, allowing π–π stacking and hydrogen bonding interactions to play a dominant role.[378] Hait *et al.*[353] reported the highest degradation efficiency for RhB at pH 8, achieving nearly complete removal within 2 h of photocatalysis using a PANI-based system. Similarly, Palliyalil *et al.*[308] employed a TiO_2@CS-PANI composite for the degradation of both MB and MO and observed maximum degradation at pH 11 for MB and pH 3 for MO. These observations clearly establish that anionic pollutants generally favour acidic conditions, where PANI is protonated and electrostatic attraction is the dominant force. In contrast, cationic pollutants exhibit enhanced degradation under neutral to alkaline conditions, where non-electrostatic interactions such as π–π stacking and hydrogen bonding become more effective.

Moreover, the role of the pK_a of a pollutant becomes particularly important in this context, as it governs the charge state of its functional groups under specific reaction

Open Access Article. Published on 12 February 2026. Downloaded on 3/23/2026 6:55:17 AM.
This article is licensed under a Creative Commons Attribution 3.0 Unported Licence.

conditions.[379] When the operating pH is close to the pK_a value, the pollutant can exist in multiple charge states, leading to dynamic interactions with the catalyst surface. Depending on the surface charge of the PANI-based composite, this behaviour may either promote effective adsorption and degradation or, conversely, hinder the photocatalytic process. Therefore, carefully aligning the solution pH with both the pollutant pK_a and the protonation state of PANI is essential for achieving the optimal photocatalytic performance.

8.2. Influence of coexisting ions and the water matrix

As evident from several studies on the photocatalytic degradation of organic pollutants, the presence of coexisting ions in aqueous solutions adversely affects the process.[127] Generally, these ions interfere with the adsorption of the pollutant over the composite and also potentially quench the ROS generated in the photocatalysis process.[17] For example, Ag_3PO_4/PANI/Cr:$SrTiO_3$ provided 100% degradation of RhB and phenol, showing negligible effects with monovalent Na^+, NO_3^- and SO_4^{2-} ions, while encountering strong interference from Cl^- and CO_3^{2-}, ascribed to the trapping of h^+ and $^{\bullet}OH$.[325] Moreover, a study conducted by Qi *et al.* revealed the significant impact of $H_2PO_4^-$ and SO_4^{2-} on the removal rate of negatively charged Cr(VI), attributed to the competitive adsorption of coexisting anions during the photocatalytic process, strongly competing for positively charged active sites of Cu/PANI/NH_2-MIL-125 (Ti) due to their valence charge and hydration characteristics.[128] The removal efficiency of Cr(VI) over CP-125(Ti) dropped but consistently remained at 84% across different water matrices (pure, tap, and lake water), highlighting its practical stability.[128]

9. Stability and reusability

The reusability of a photocatalyst is a crucial factor in maintaining its photocatalytic ability, and its cost-effectiveness also matters.[129,311,380] Several studies on PANI-based ternary composites have shown potential results regarding stability and reusability. Mitra *et al.*[311] investigated the stability of 22 wt% Al-doped zinc oxide-PANI up to 5 repetitive cycles by recycling the catalyst with a significant degradation efficiency. Pure PANI also displayed photostability and reproducibility with a degradation efficiency of 85.61% for the removal of MB even after 5 cycles under simulated sunlight.[68] PANI-supported MWCNTs/ZnO/Ag_2CO_3 is also tested up to 5 cycles, which showed an efficiency of 49.78%, indicating significant reusability.[381] Similarly, after 5 successive cycles, Hu/PANI@Ni_2O_3 showed excellent stability and retained 84.5% of the initial degradation efficiency for Safranin-T dye.[294] The g-C_3N_4/TiO_2@PANI composite displayed 90% photocatalytic degradation efficiency for the Congo red dye even after 4 successive cycles, which is attributed to the wider visible light absorption of the photocatalyst and the sensitizing effect of g-C_3N_4 and PANI.[382] Moreover, 0.5%PANI@Bi_2O_3–BiOCl, when evaluated, displayed a drop of only 10% in the initial photocatalytic degradation efficiency after up to 4 consecutive runs for the removal of the MB dye.[348] These studies highlight that PANI and PANI-based photocatalysts show high efficiency, stability, and reproducibility, which make them suitable for practical field applications. Moreover, further studies should be conducted to discover greener and more cost-efficient methods for catalyst regeneration.

10. Sustainability aspects of PANI-based composites

PANI-based ternary photocatalysts are promising materials for achieving sustainable wastewater treatment, primarily due to their facile and low-cost synthesis, tunable physicochemical properties, and environmental compatibility.[69] The studies discussed in the previous sections demonstrated that integrating conducting polymers with a wide range of functional materials can reduce reliance on artificial UV-driven energy sources and significantly enhance the overall energy efficiency.[383] If we start from the synthesis perspective, several green fabrication strategies have been developed to reduce chemical consumption and energy input.[384] These approaches include aqueous-phase polymerization, the use of mild oxidants and organic acid dopants, enzymatic routes, and room-temperature synthesis procedures. In addition, the overall energy footprint can be further reduced by incorporating earth-abundant co-catalysts and bio-based templates that act as natural carbon sources, such as chitosan, cellulose, and lignin.

A limited number of studies have also investigated the eco-toxicity of PANI-based composites. Notably, Zhao *et al.*[383] evaluated the virotoxicity of a BVGT–PANI composite against *Bacillus subtilis* and *Staphylococcus aureus*, and their results showed no observable inhibition zones, indicating negligible antibacterial toxicity. Similarly, Barik *et al.*[385] assessed the cytotoxicity of a polyaniline-$ZnWO_4$-WO_3 (PZW) photocatalyst using *Drosophila melanogaster* larvae as a model organism and consistently reported non-toxic effects. Therefore, it demonstrates the non-toxic nature of PANI-based composites. Interestingly, these approaches were further validated by Galloni *et al.*,[386] who performed a comparative life cycle assessment and demonstrated that process scale-up can significantly enhance both efficiency and sustainability by adopting alternative green synthesis strategies and optimizing electrical energy consumption during synthesis. In addition, the sustainability of PANI-based composites is further enhanced by their chemical and structural stability. Many studies report stable photocatalytic performance over multiple reaction cycles, indicating good reusability and resistance to photocorrosion. Therefore, PANI-based ternary photocatalysts represent a sustainable and worthwhile platform for wastewater treatment, combining green synthesis, low toxicity, structural stability, and long-term reusability, which collectively support their potential for scalable and environmentally responsible photocatalytic applications.

11. Challenges and future recommendations

The studies discussed in previous sections showed that PANI plays a major role in the degradation of various organic

 © 2026 The Author(s). Published by the Royal Society of Chemistry

Open Access Article. Published on 12 February 2026. Downloaded on 3/23/2026 6:55:17 AM.
This article is licensed under a Creative Commons Attribution 3.0 Unported Licence.

pollutants. However, the conventional polymerization in the synthetic route employs strong oxidants such as APS, HCl, H_2SO_4 and organic dopants, producing effluents with low pH, which limits the green chemistry approach. Several composites show uneven interfacial bonding, resulting in weaker interactions, leading to agglomeration, active site blockage, and discontinuous charge transfer. PANI experiences photobleaching and exhibits pH-dependent conductivity in actual wastewater, restricting the long-term stability, and excessive PANI loading hinders light penetration and obstructs active sites. Moreover, several studies were mainly focused on single-pollutant systems in DI water (ideal condition), overlooking the effect of co-existing ions, organic/inorganic matter, and variable pH. These factors strongly interfere with the degradation efficiencies and overall reaction kinetics. Furthermore, the powdered composites have a poor recovery rate and also require energy-intensive procedures, which increases the operational cost and restricts scalability. Moreover, the incomplete assessment of toxic degradation by products, catalyst leaching and effluent pathways can cause secondary pollution, which could be hazardous. The photocatalyst immobilization, uniform light distribution, hydraulic management, and engineered reactor characteristics are major hurdles for transforming PANI's application to pilot scale or industrial level.

To address the above-mentioned issues, further studies should be conducted to prioritise minimal chemical waste, reduced energy consumption, and comparatively environmentally friendly routes. The adoption of greener oxidants like enzymatic or electrochemical oxidants, mild organic acids, bio-derived dopants, and aqueous or solvent-free polymers will reduce the environmental burden. Moreover, the toxic co-catalyst should be eliminated and replaced with earth-abundant elements. The synthesis reactions at lowered temperatures should be preferred. The innovations in PANI-based composites should be directed towards ligand inclusion with advancements in intrinsic properties or modifications in chemical structures supported with active functional groups. These approaches may lead to a sustained real scenario of variable pH, ensuring better charge mobility, thereby enhancing the efficiency. Long-term stability against overoxidation and photobleaching can be enhanced through cross-linking strategies and protective thin coating. Magnetic PANI-based composites may offer separation and catalyst recovery. Major attention should be paid to the material recovery without escalation in operational cost. The fouling, deactivation of catalysts, mechanical abrasion, loss of activity in real water due to variable pH and the presence of organic/inorganic matter, and chemical instability should be addressed by the immobilization of photocatalysts over substrates, such as glass fibres, metal foams, 3D printed materials, and metal meshes. Furthermore, the integration of machine learning (ML) should be done in data-driven optimization. Strategies such as the integration of ML for optimization, sensor-based feedback control, and forecasting reactor performance reduce resource consumption, make the process cost-efficient and minimise energy use. There is also a need for modelling to determine the best possible quantity and conditions required for the catalyst to utilize the full spectrum of light source, E_g, and other important factors. Real-time monitoring of the pollutant concentration and interferences in the wastewater is needed for quantifying maximum and efficient removal. The studies should be forwarded for the photocatalytic membrane reactors (PMRs), flow-through photocatalytic reactors (FTPRs), and hybrid treatment modules. Hence, various reactor designs should be explored for the pilot-scale demonstrations. Moreover, hybrid or integrated treatment systems must be further explored, like a combination of biological and photocatalytic reactors, such that other pollutants can be removed to reduce the load on the photocatalytic reactor, which thereby increases the efficiency. A comprehensive life cycle assessment of the material should be conducted, including the end-of-life stage of the photocatalyst. The eco-toxicity assessment of the material and the degradation by-product should be carried out for further strengthening their practical reusability.

12. Conclusions

PANI and its ternary-based composite have garnered significant attention owing to their simple synthesis, electrical conductivity, and structural stability. This paper examines the structure and properties of PANI, discusses various synthesis methods for PANI and its ternary composites, elucidates the role of PANI in these systems, and presents suitable materials for effective composite formation with PANI. Various parameters such as temperature, pH conditions, protonic acids, oxidants, and specific templates, influencing the synthetic routes and morphology of the resulting product, have been discussed. Moreover, the review explains the photocatalytic mechanism in PANI-based ternary composites, clarifying the purpose and functional role of incorporating PANI into the ternary systems. The findings confirmed that PANI-based ternary composites were highly effective in degrading dyes, PhACs, phenolics, and xenobiotics and reducing heavy metals, due to the enhanced light absorption ability, efficient charge separation, and the presence of delocalized electrons. Furthermore, the PANI-based ternary photocatalyst demonstrated remarkable stability and reusability after multiple cycles of reuse. The review highlights the necessity of developing green synthetic methods to mitigate environmental impacts. These methods can improve the sustainability, safety, and scalability of PANI-based photocatalysts. Overall, this review highlights the potential of PANI-based ternary composites as effective and durable photocatalysts for environmental remediation applications.

Author contributions

Jyoti Kumari: writing – original draft, validation, methodology, investigation, formal analysis, data curation, and conceptualization. Adarsh Singh: writing – original draft, validation, methodology, investigation, formal analysis, data curation, and conceptualization. Akash Rawat: writing – original draft, validation, methodology, investigation, formal analysis, data curation, and conceptualization. Suneel Kumar Srivastava: writing –

Open Access Article. Published on 12 February 2026. Downloaded on 3/23/2026 6:55:17 AM. This article is licensed under a Creative Commons Attribution 3.0 Unported Licence.

review and editing, visualization, supervision, methodology, and conceptualization. Ashok Kumar Gupta: writing – review and editing, visualization, supervision, methodology, and conceptualization.

Conflicts of interest

There are no conflicts of interest to declare.

List of abbreviations

$[Ru(bipy)_3]^{2+}$	Tris(bipyridine)ruthenium(II) chloride
AOPs	Advanced oxidation processes
APS	Ammonium persulfate
CB	Conduction band
CECs	Contaminants of emerging concerns
CNTs	Carbon nanotubes
CR	Congo red
CSA	Camphor sulfonic acid
ECP	Electrochemical polymerization
ECs	Emerging contaminants
EDCs	Endocrine-disrupting chemicals
EDTA	Ethylenediaminetetraacetic acid
E_f	Fermi level
E_g	Band gap
EIS	Electrochemical impedance spectroscopy
EM	Emeraldine
EPs	Emerging pollutants
ESI-MS	Electrospray ionization-mass spectrometry
GO	Graphene oxide
HOMO	Highest occupied molecular orbital
HRP	Horseradish peroxidase
IEF	Internal electric field
LUMO	Lowest unoccupied molecular orbital
MB	Methylene blue
MO	Methyl orange
MPs	Micropollutants
MV^{2+}	Methylviologen
NA	Nigraniline
Nd:YAG	Neodymium-doped yttrium aluminium garnet
NIR	Near-infrared
OP	Oxidation photocatalyst
PAHs	Polycyclic aromatic hydrocarbons
PANI	Polyaniline
PEDOT	Poly(3,4-ethylenedioxythiophene)
PET	Polyethylene terephthalate
PhACs	Pharmaceutically active compounds
PI	Polyimide
PNA	Pernigraniline
PPCPs	Pharmaceuticals and personal care products
PS	Polystyrene
PSS	Polystyrene sulfonate
PVC	Polyvinyl chloride
rGO	Reduced graphene oxide
RhB	Rhodamine B
ROS	Reactive oxygen species
RP	Reduction photocatalyst
TrOCs	Trace organic compounds
UV	Ultraviolet
VB	Valence band

Data availability

The data that support the findings of this study are available from the corresponding author upon reasonable request.

Supplementary information (SI) is available. See DOI: https://doi.org/10.1039/d5su00570a.

Acknowledgements

Jyoti Kumari, Adarsh Singh, and Akash Rawat are thankful to the Indian Institute of Technology Kharagpur, India, for the financial support. Suneel Kumar Srivastava (Retired Professor), former faculty in the Department of Chemistry, Indian Institute of Technology Kharagpur, also remains very appreciative for making this effort possible.

References

1 A. Singh, A. Majumder, D. Saidulu, A. Bhattacharya, A. Bhatnagar and A. K. Gupta, *J. Environ. Manage.*, 2024, **354**, 120339.
2 N. H. Tran and K. Y. H. Gin, *Sci. Total Environ.*, 2017, **599–600**, 1503–1516.
3 X. Lin, J. Xu, A. A. Keller, L. He, Y. Gu, W. Zheng, D. Sun, Z. Lu, J. Huang, X. Huang and G. Li, *Sci. Total Environ.*, 2020, **744**, 140977.
4 A. Singh, A. Srivastava, D. Saidulu and A. K. Gupta, *J. Environ. Manage.*, 2022, **317**, 115305.
5 A. Gogoi, P. Mazumder, V. K. Tyagi, G. G. Tushara Chaminda, A. K. An and M. Kumar, *Groundw. Sustain. Dev.*, 2018, **6**, 169–180.
6 J. M. Philip, U. K. Aravind and C. T. Aravindakumar, *Chemosphere*, 2018, **190**, 307–326.
7 B. Díaz-Garduño, M. G. Pintado-Herrera, M. Biel-Maeso, J. J. Rueda-Márquez, P. A. Lara-Martín, J. A. Perales, M. A. Manzano, C. Garrido-Pérez and M. L. Martín-Díaz, *Water Res.*, 2017, **119**, 136–149.
8 G. Lofrano, G. Libralato, S. Meric, V. Vaiano, O. Sacco, V. Venditto, M. Guida and M. Carotenuto, in *Visible Light Active Structured Photocatalysts for the Removal of Emerging Contaminants*, Elsevier, 2020, pp. 1–25.
9 T. Deblonde, C. Cossu-Leguille and P. Hartemann, *Int. J. Hyg. Environ. Health*, 2011, **214**, 442–448.
10 L. Rizzo, S. Malato, D. Antakyali, V. G. Beretsou, M. B. Đolić, W. Gernjak, E. Heath, I. Ivancev-Tumbas, P. Karaolia, A. R. Lado Ribeiro, G. Mascolo, C. S. McArdell, H. Schaar, A. M. T. Silva and D. Fatta-Kassinos, *Sci. Total Environ.*, 2019, **655**, 986–1008.
11 C. Grandclément, I. Seyssiecq, A. Piram, P. Wong-Wah-Chung, G. Vanot, N. Tiliacos, N. Roche and P. Doumenq, *Water Res.*, 2017, **111**, 297–317.
12 S. K. Srivastava, *RSC Appl. Interfaces*, 2024, **1**, 340–429.
13 A. Singh, A. Bhatnagar and A. K. Gupta, *Sep. Purif. Technol.*, 2025, 132176.

 © 2026 The Author(s). Published by the Royal Society of Chemistry

Open Access Article. Published on 12 February 2026. Downloaded on 3/23/2026 6:55:17 AM. This article is licensed under a Creative Commons Attribution 3.0 Unported Licence.

14 A. Singh, A. Bhatnagar and A. K. Gupta, *J. Environ. Chem. Eng.*, 2024, **12**, 114192.
15 S. Dutta, B. Gupta, S. K. Srivastava and A. K. Gupta, *Mater. Adv.*, 2021, **2**, 4497–4531.
16 A. K. Gupta, A. Singh, D. Saidulu, A. Srivastava and A. Rawat, in *Biodegradation of Toxic and Hazardous Chemicals*, CRC Press, Boca Raton, 2024, pp. 120–149.
17 A. Rawat, S. K. Srivastava, C. S. Tiwary and A. K. Gupta, *J. Environ. Chem. Eng.*, 2024, **12**, 112879.
18 A. Rawat, S. K. Srivastava, C. S. Tiwary and A. K. Gupta, *J. Mater. Chem. A*, 2025, **13**, 1271–1286.
19 A. Rawat, A. Srivastava, A. Bhatnagar and A. K. Gupta, *J. Cleaner Prod.*, 2023, **383**, 135382.
20 A. Singh, S. K K, A. Bhatnagar and A. K. Gupta, *Sep. Purif. Technol.*, 2025, **353**, 128588.
21 J. Roberts, A. Kumar, J. Du, C. Hepplewhite, D. J. Ellis, A. G. Christy and S. G. Beavis, *Sci. Total Environ.*, 2016, **541**, 1625–1637.
22 R. Naidu, V. A. Arias Espana, Y. Liu and J. Jit, *Chemosphere*, 2016, **154**, 350–357.
23 J. O. Tijani, O. O. Fatoba, O. O. Babajide and L. F. Petrik, *Environ. Chem. Lett.*, 2016, **14**, 27–49.
24 R. M. Rego, G. Kuriya, M. D. Kurkuri and M. Kigga, *J. Hazard. Mater.*, 2021, **403**, 123605.
25 J. Annamalai and V. Namasivayam, *Environ. Int.*, 2015, **76**, 78–97.
26 A. Saravanan, P. S. Kumar, S. Jeevanantham, M. Anubha and S. Jayashree, *Environ. Pollut.*, 2022, **298**, 118844.
27 S. Dutta, S. K. Banu and J. A. Arosh, *Reprod. Toxicol.*, 2023, **115**, 56–73.
28 A. Ruhí, V. Acuña, D. Barceló, B. Huerta, J.-R. Mor, S. Rodríguez-Mozaz and S. Sabater, *Sci. Total Environ.*, 2016, **540**, 250–259.
29 C. Sheng, A. G. A. Nnanna, Y. Liu and J. D. Vargo, *Sci. Total Environ.*, 2016, **550**, 1075–1083.
30 J. Gomes, R. Costa, R. M. Quinta-Ferreira and R. C. Martins, *Sci. Total Environ.*, 2017, **586**, 265–283.
31 S. Arzate, J. L. García Sánchez, P. Soriano-Molina, J. L. Casas López, M. C. Campos-Mañas, A. Agüera and J. A. Sánchez Pérez, *Chem. Eng. J.*, 2017, **316**, 1114–1121.
32 P. R. Rout, T. C. Zhang, P. Bhunia and R. Y. Surampalli, *Sci. Total Environ.*, 2021, **753**, 141990.
33 A. K. Gupta and S. Ayoob, *Fluoride in Drinking Water: Status, Issues, and Solutions*, CRC Press, 2016.
34 A. Mirzaei, Z. Chen, F. Haghighat and L. Yerushalmi, *Chemosphere*, 2017, **174**, 665–688.
35 N. Klamerth, S. Malato, M. I. Maldonado, A. Agüera and A. R. Fernández-Alba, *Environ. Sci. Technol.*, 2010, **44**, 1792–1798.
36 G. Ferro, M. I. Polo-López, A. B. Martínez-Piernas, P. Fernández-Ibáñez, A. Agüera and L. Rizzo, *Environ. Sci. Technol.*, 2015, **49**, 11096–11104.
37 C. Byrne, G. Subramanian and S. C. Pillai, *J. Environ. Chem. Eng.*, 2018, **6**, 3531–3555.
38 S. A. Fast, V. G. Gude, D. D. Truax, J. Martin and B. S. Magbanua, *Environ. Processes*, 2017, **4**, 283–302.
39 R. Molinari, C. Lavorato and P. Argurio, *Catal. Today*, 2017, **281**, 144–164.
40 M. N. Chong, B. Jin, C. W. K. Chow and C. Saint, *Water Res.*, 2010, **44**, 2997–3027.
41 R. Ameta and S. C. Ameta, *Photocatalysis*, CRC Press, 2016.
42 V. K. Parida, S. K. Srivastava, A. K. Gupta and A. Rawat, *Mater. Express*, 2023, **13**, 1–38.
43 M. Ni, M. K. H. Leung, D. Y. C. Leung and K. Sumathy, *Renewable Sustainable Energy Rev.*, 2007, **11**, 401–425.
44 W. Chen, L. Ni, K. Ogino, H. Sun, J. Bi and H. Hou, *Coatings*, 2025, **15**, 32.
45 B. Liu, Z. Luo, W. Wu, Y. Qi, Y. Qin and X. Qiu, *Carbon Res.*, 2025, **4**, 26.
46 N. Askari, M. Jamalzadeh, A. Askari, N. Liu, B. Samali, M. Sillanpaa, L. Sheppard, H. Li and R. Dewil, *J. Environ. Sci.*, 2025, **148**, 283–297.
47 G. Iervolino, I. Zammit, V. Vaiano and L. Rizzo, *Top. Curr. Chem.*, 2020, **378**, 7.
48 X. Pei, J. Bian, W. Zhang, Z. Hu, Y. H. Ng, Y. Dong, X. Zhai, Z. Wei, Y. Liu, J. Deng, H. Dai and L. Jing, *Adv. Funct. Mater.*, 2024, **34**, 2400542.
49 H. Dong, G. Zeng, L. Tang, C. Fan, C. Zhang, X. He and Y. He, *Water Res.*, 2015, **79**, 128–146.
50 S. Mohana Roopan and M. A. Khan, *Catal. Rev.*, 2023, **65**, 620–693.
51 Y. Yuan, G.-F. Huang, W.-Y. Hu, D.-N. Xiong, B.-X. Zhou, S. Chang and W.-Q. Huang, *J. Phys. Chem. Solids*, 2017, **106**, 1–9.
52 Z. Liu, K. Xu, H. Yu, M. Zhang and Z. Sun, *Appl. Surf. Sci.*, 2021, **545**, 148986.
53 N. K and C. S. Rout, *RSC Adv.*, 2021, **11**, 5659–5697.
54 H. O. Shoyiga and O. E. Fayemi, *Heliyon*, 2025, **11**, e41575.
55 S. K. Srivastava, *RSC Appl. Polym.*, 2026, **4**, 120–199.
56 A. Taghizadeh, M. Taghizadeh, M. Jouyandeh, M. K. Yazdi, P. Zarrintaj, M. R. Saeb, E. C. Lima and V. K. Gupta, *J. Mol. Liq.*, 2020, **312**, 113447.
57 U. Riaz, S. M. Ashraf and J. Kashyap, *Polym.-Plast. Technol. Eng.*, 2015, **54**, 1850–1870.
58 G. Saianand, A.-I. Gopalan, L. Wang, K. Venkatramanan, V. A. L. Roy, P. Sonar, D.-E. Lee and R. Naidu, *Environ. Technol. Innovation*, 2022, **28**, 102698.
59 E. M. Geniès, A. Boyle, M. Lapkowski and C. Tsintavis, *Synth. Met.*, 1990, **36**, 139–182.
60 A. F. Diaz, J. I. Castillo, J. A. Logan and W.-Y. Lee, *J. Electroanal. Chem. Interfacial Electrochem.*, 1981, **129**, 115–132.
61 L. V. Kayser and D. J. Lipomi, *Adv. Mater.*, 2019, **31**, 1806133.
62 T. P. Kaloni, P. K. Giesbrecht, G. Schreckenbach and M. S. Freund, *Chem. Mater.*, 2017, **29**, 10248–10283.
63 B. Hudson, *Materials*, 2018, **11**, 242.
64 M. J. González-Tejera, E. S. de la Blanca and I. Carrillo, *Synth. Met.*, 2008, **158**, 165–189.
65 C. Ambrosch-Draxl, J. A. Majewski, P. Vogl and G. Leising, *Phys. Rev. B:Condens. Matter Mater. Phys.*, 1995, **51**, 9668–9676.

Open Access Article. Published on 12 February 2026. Downloaded on 3/23/2026 6:55:17 AM.
This article is licensed under a Creative Commons Attribution 3.0 Unported Licence.

66 S. Goswami, S. Nandy, E. Fortunato and R. Martins, *J. Solid State Chem.*, 2023, **317**, 123679.
67 K. Zhang, Z. Wang, X. Liu, G. Yang, C. Jiang, Z. Pan, X. Liu, Y. Wang and B. Xing, *Environ. Sci.:Water Res. Technol.*, 2024, **10**, 376–388.
68 C. Van Tran, D. Van Lai, T. M. Nguyen, X. Quynh Thi Le, H. H. Nguyen, N. T. M. Quan, T. T. Nguyen and D. D. La, *Nanoscale Adv.*, 2025, **7**, 800–807.
69 P. Hait, R. Mehta and S. Basu, *New J. Chem.*, 2025, **49**, 14623–14637.
70 P. L. Meena and A. K. Surela, *J. Mol. Liq.*, 2024, **412**, 125828.
71 Y. Fu and M. Janczarek, *Crystals*, 2023, **13**, 1637.
72 A. L. Pang, A. Arsad, M. A. Ahmad Zaini, R. Garg, M. Saqlain Iqbal, U. Pal, M. A. S. Mohammad Haniff, A. Azlan Hamzah, S.-Y. Pung and M. Ahmadipour, *Chem. Eng. Commun.*, 2024, **211**, 275–299.
73 C. Prasad, H. Tang and I. Bahadur, *J. Mol. Liq.*, 2019, **281**, 634–654.
74 G. G, A. Sathish, P. S. Kumar, K. Nithya and G. Rangasamy, *Chemosphere*, 2022, **309**, 136617.
75 D. Kanakaraju and A. Chandrasekaran, *Sci. Total Environ.*, 2023, **868**, 161525.
76 E. Kang, *Prog. Polym. Sci.*, 1998, **23**, 277–324.
77 A. G. MacDiarmid and A. J. Epstein, *The Polyanilines: Recent Advances in Chemistry and Processing*, 1990, pp. 303–315.
78 Y. Chen, E. T. Kang, K. G. Neoh and K. L. Tan, *Polymer*, 2000, **41**, 3279–3287.
79 D. D. Zhou, X. T. Cui, A. Hines and R. J. Greenberg, *Conducting Polymers in Neural Stimulation Applications*, 2009, pp. 217–252.
80 M. Beygisangchin, S. Abdul Rashid, S. Shafie, A. R. Sadrolhosseini and H. N. Lim, *Polymers*, 2021, **13**, 2003.
81 N. Gospodinova and L. Terlemezyan, *Prog. Polym. Sci.*, 1998, **23**, 1443–1484.
82 B. Malhotra, C. Dhand, R. Lakshminarayanan, N. Dwivedi, S. Mishra, P. Solanki, M. Venkatesh, R. W. Beuerman and S. Ramakrishna, *Nanobiosensors Dis. Diagnosis*, 2015, 25.
83 V. Mottaghitalab, B. Xi, G. M. Spinks and G. G. Wallace, *Synth. Met.*, 2006, **156**, 796–803.
84 M. Wan, W. Zhou, Y. Li and J. Liu, *Solid State Commun.*, 1992, **81**, 313–316.
85 S. Khasim, S. C. Raghavendra, M. Revanasiddappa, K. C. Sajjan, M. Lakshmi and M. Faisal, *Bull. Mater. Sci.*, 2011, **34**, 1557–1561.
86 P. Kaushik, R. Bharti, R. Sharma, M. Verma, R. T. Olsson and A. Pandey, *Eur. Polym. J.*, 2024, **221**, 113574.
87 A. H. Majeed, L. A. Mohammed, O. G. Hammoodi, S. Sehgal, M. A. Alheety, K. K. Saxena, S. A. Dadoosh, I. K. Mohammed, M. M. Jasim and N. U. Salmaan, *Int. J. Polym. Sci.*, 2022, **2022**, 1–19.
88 W. Hai, C. Chen, Q. Yu, M. Li, Z. Jiang, H. Shao, G. Shao, J. Jiang, N. Chen and S. Bi, *Appl. Surf. Sci.*, 2023, **637**, 157975.
89 Y. Kang, H. Lee, J. Namgoong, B. Jung and H. Lee, *Polymer*, 1999, **40**, 2209–2213.
90 A. L. Kon'kin, V. G. Shtyrlin, R. R. Garipov, A. V. Aganov, A. V. Zakharov, V. I. Krinichnyi, P. N. Adams and A. P. Monkman, *Phys. Rev. B:Condens. Matter Mater. Phys.*, 2002, **66**, 075203.
91 Z. Li and L. Gong, *Materials*, 2020, **13**, 548.
92 V. Babel and B. L. Hiran, *Polym. Compos.*, 2021, **42**, 3142–3157.
93 X. Chen, C. A. Yuan, C. K. Y. Wong, H. Ye, S. Y. Y. Leung and G. Zhang, *Sens. Actuators, B*, 2012, **174**, 210–216.
94 W.-S. Huang, B. D. Humphrey and A. G. MacDiarmid, *J. Chem. Soc., Faraday Trans.*, 1986, **82**, 2385.
95 N. Khalid, J. A. Razak, H. Hasib, M. Ismail, N. Mohamad, R. Junid and P. Puspitasari, *IOP Conf. Ser.:Mater. Sci. Eng.*, 2020, **957**, 012028.
96 S. K. Singh, R. Shukla and C. Dixit, *Int. J. Phys. Appl.*, 2022, **4**, 01–06.
97 C. Zhao, K. Gao, C. Ma, M. Wu, K. Cao, Y. Yang, C. Hong and X. Qiao, *J. Mol. Struct.*, 2020, **1209**, 127924.
98 W. S. Huang and A. G. MacDiarmid, *Polymer*, 1993, **34**, 1833–1845.
99 C. Barbero and R. Kötz, *J. Electrochem. Soc.*, 1994, **141**, 859–865.
100 Y. Xia, J. M. Wiesinger, A. G. MacDiarmid and A. J. Epstein, *Chem. Mater.*, 1995, **7**, 443–445.
101 S. Mahalakshmi and V. Sridevi, *Mater. Chem. Phys.*, 2019, **235**, 121728.
102 J. Stejskal, P. Kratochvíl and N. Radhakrishnan, *Synth. Met.*, 1993, **61**, 225–231.
103 J. Yu, Y. Liu, H. Wang, Q. Yan and J. Luo, *Environ. Sci.:Water Res. Technol.*, 2023, **9**, 406–418.
104 K. Jlassi, A. B. Radwan, K. K. Sadasivuni, M. Mrlik, A. M. Abdullah, M. M. Chehimi and I. Krupa, *Sci. Rep.*, 2018, **8**, 13369.
105 M. Sababi, J. Pan, P.-E. Augustsson, P.-E. Sundell and P. M. Claesson, *Corros. Sci.*, 2014, **84**, 189–197.
106 A. A. Ganash, F. M. Al-Nowaiser, S. A. Al-Thabaiti and A. A. Hermas, *Prog. Org. Coat.*, 2011, **72**, 480–485.
107 K. Kamaraj, V. Karpakam, S. Sathiyanarayanan, S. S. Azim and G. Venkatachari, *Electrochim. Acta*, 2011, **56**, 9262–9268.
108 A. Mirmohseni and A. Oladegaragoze, *Synth. Met.*, 2000, **114**, 105–108.
109 S. Chaudhari and P. P. Patil, *Electrochim. Acta*, 2011, **56**, 3049–3059.
110 S. Bhadra, D. Khastgir, N. K. Singha and J. H. Lee, *Prog. Polym. Sci.*, 2009, **34**, 783–810.
111 N. Sharma, A. Singh, N. Kumar, A. Tiwari, M. Lal and S. Arya, *J. Mater. Sci.*, 2024, **59**, 6206–6244.
112 J. Hao, L. Wang, X. Wang, J. Wang, M. He, X. Zhang, J. Wang, L. Nie and J. Li, *Environ. Sci.:Water Res. Technol.*, 2024, **10**, 105–127.
113 F. Alzoubi, M. Al-Gharram, T. AlZoubi, O. A. Noqta, G. Makhadmeh, H. Al-Khateeb and M. Al-Qadi, *Ceram. Int.*, 2024, **50**, 37968–37977.
114 M. Al-Gharram and T. AlZoubi, *Ceram. Int.*, 2024, **50**, 32841–32852.

 © 2026 The Author(s). Published by the Royal Society of Chemistry

Open Access Article. Published on 12 February 2026. Downloaded on 3/23/2026 6:55:17 AM.
This article is licensed under a Creative Commons Attribution 3.0 Unported Licence.

115 L. George, *Mater. Today: Proc.*, 2023, DOI: 10.1016/j.matpr.2023.01.417.
116 J. Liu, D. Zheng, W. Chang, F. Deng and D. Liu, *J. Appl. Polym. Sci.*, 2025, **142**, e56483.
117 A. Balboa-Palomino, U. Páramo-García, J. A. Melo-Banda, J. Y. Verde-Gómez and N. V. Gallardo-Rivas, *Polymers*, 2024, **16**, 1677.
118 S. Jamali Alyani, A. Dadvand Koohi, S. S. Ashraf Talesh and A. Ebrahimian Pirbazari, *Environ. Sci. Pollut. Res.*, 2024, **31**, 42521–42546.
119 A. Muhammad, A.-H. A. Shah, S. Bilal and G. Rahman, *Materials*, 2019, **12**, 1764.
120 A. Helal, A. M. S. Salem and S. I. El-Hout, *J. Photochem. Photobiol., A*, 2024, **447**, 115232.
121 Y. Zhang, Y. Gao, R. Deng, Z. Qin, F. Shi, J. Zeng, C. Zhao, Y. Pu and T. Duan, *Sep. Purif. Technol.*, 2025, **354**, 129331.
122 E. Wu, J. Zhang, M. Cai, J. Bai, J. Xue, Y. Jiang, J. Chen, C.-J. Mao and S. Sun, *Sep. Purif. Technol.*, 2025, **354**, 129250.
123 A. Jeyaranjan, T. S. Sakthivel, C. J. Neal and S. Seal, *Carbon*, 2019, **151**, 192–202.
124 E. Spain, T. E. Keyes and R. J. Forster, *J. Electroanal. Chem.*, 2013, **711**, 38–44.
125 M. Malekzadeh and M. T. Swihart, *Chem. Soc. Rev.*, 2021, **50**, 7132–7249.
126 G. Mandal, J. Bauri, D. Nayak, S. Kumar, S. Ansari and R. Bilash Choudhary, in *Trends and Developments in Modern Applications of Polyaniline*, IntechOpen, 2023.
127 A. Rawat, R. B. de Oliveira, T. Pal, K. A. L. Lima, G. S. L. Fabris, R. M. Tromer, M. L. Pereira Junior, A. Singh, A. K. Gupta, D. S. Galvão and C. S. Tiwary, *J. Mater. Chem. A*, 2026, **14**, 2871–2883.
128 P. Qi, Z. Wang, X. Zhou, X. Zhang, S. Zhou, F. Yang, Q. Xu, Z. Liu, Z. Zhang and L. Zeng, *Process Saf. Environ. Prot.*, 2025, **201**, 107497.
129 L. Jing, Y. Xu, M. Xie, J. Liu, J. Deng, L. Huang, H. Xu and H. Li, *Chem. Eng. J.*, 2019, **360**, 1601–1612.
130 L. A. Samuelson, A. Anagnostopoulos, K. S. Alva, J. Kumar and S. K. Tripathy, *Macromolecules*, 1998, **31**, 4376–4378.
131 A. Jabłońska, M. Gniadek and B. Pałys, *J. Phys. Chem. C*, 2015, **119**, 12514–12522.
132 S.-C. Kim, P. Huh, J. Kumar, B. Kim, J.-O. Lee, F. F. Bruno and L. A. Samuelson, *Green Chem.*, 2007, **9**, 44–48.
133 J.-Y. Kim, J.-H. Lee and S.-J. Kwon, *Synth. Met.*, 2007, **157**, 336–342.
134 B. Das, S. Kar, S. Chakraborty, D. Chakraborty and S. Gangopadhyay, *J. Appl. Polym. Sci.*, 1998, **69**, 841–844.
135 A. T. Lawal and G. G. Wallace, *Talanta*, 2014, **119**, 133–143.
136 Y. Gao, Z.-H. Kang, X. Li, X.-J. Cui and J. Gong, *CrystEngComm*, 2011, **13**, 3370.
137 S. V. Joana Sury, A. Ulianas and S. Aini, *J. Phys.: Conf. Ser.*, 2021, **1788**, 012004.
138 K. Teshima, S. Uemura, N. Kobayashi and R. Hirohashi, *Macromolecules*, 1998, **31**, 6783–6788.
139 M. R. Gizdavic-Nikolaidis, D. R. Stanisavljev, A. J. Easteal and Z. D. Zujovic, *Macromol. Rapid Commun.*, 2010, **31**, 657–661.
140 J. F. Felix, R. A. Barros, W. M. de Azevedo and E. F. da Silva, *Synth. Met.*, 2011, **161**, 173–176.
141 T. Ishioka, T. Uchida and N. Teramae, *Chem. Lett.*, 1998, **27**, 765–766.
142 Y. Kim, S. Fukai and N. Kobayashi, *Synth. Met.*, 2001, **119**, 337–338.
143 M. Bláha, M. Trchová, P. Bober, Z. Morávková, J. Prokeš and J. Stejskal, *Mater. Chem. Phys.*, 2017, **194**, 206–218.
144 X. Zheng, M. E. Ali Mohsin, A. Arsad and A. Hassan, *J. Appl. Polym. Sci.*, 2021, **138**, 50637.
145 X. Liu, W. Zhou, X. Qian, J. Shen and X. An, *Carbohydr. Polym.*, 2013, **92**, 659–661.
146 P. Bober, J. Stejskal, M. Trchová and J. Prokeš, *Polymer*, 2011, **52**, 5947–5952.
147 J. Stejskal, M. Exnerová, Z. Morávková, M. Trchová, J. Hromádková and J. Prokeš, *Polym. Degrad. Stab.*, 2012, **97**, 1026–1033.
148 H. Yan and N. Toshima, *Synth. Met.*, 1995, **69**, 151–152.
149 M. Omastová, K. Mosnáčková, M. Trchová, E. N. Konyushenko, J. Stejskal, P. Fedorko and J. Prokeš, *Synth. Met.*, 2010, **160**, 701–707.
150 Y. Wang, X. Jing and J. Kong, *Synth. Met.*, 2007, **157**, 269–275.
151 M. Neetika, J. Rajni, P. K. Singh, B. Bhattacharya, V. Singh and S. Tomar, *High Perform. Polym.*, 2017, **29**, 266–271.
152 R. Hirase, T. Shikata and M. Shirai, *Synth. Met.*, 2004, **146**, 73–77.
153 M. S. Zoromba, S. Alghool, S. M. S. Abdel-Hamid, M. Bassyouni and M. H. Abdel-Aziz, *Polym. Adv. Technol.*, 2017, **28**, 842–848.
154 M. M. Ayad and M. A. Shenashin, *Eur. Polym. J.*, 2004, **40**, 197–202.
155 M. P. Sidheekha, K. Nufaira, A. K. Shabeeba, L. Rajan and Y. A. Ismail, *Mater. Today: Proc.*, 2022, **51**, 2286–2292.
156 U. S. Waware and S. S. Umare, *React. Funct. Polym.*, 2005, **65**, 343–350.
157 K. Tzou and R. V. Gregory, *Synth. Met.*, 1992, **47**, 267–277.
158 G. G. Wallace, P. R. Teasdale, G. M. Spinks and L. A. P. Kane-Maguire, *Conductive Electroactive Polymers*, CRC Press, 2008.
159 A. Dan and P. K. Sengupta, *J. Appl. Polym. Sci.*, 2004, **91**, 991–999.
160 E. Erdem, M. Karakışla and M. Saçak, *Eur. Polym. J.*, 2004, **40**, 785–791.
161 N. V. Blinova, J. Stejskal, M. Trchová, J. Prokeš and M. Omastová, *Eur. Polym. J.*, 2007, **43**, 2331–2341.
162 W. Shen, H. Deng and Z. Gao, *RSC Adv.*, 2014, **4**, 53257–53264.
163 R. A. Gross, A. Kumar and B. Kalra, *Chem. Rev.*, 2001, **101**, 2097–2124.
164 W. Liu, J. Kumar, S. Tripathy and L. A. Samuelson, *Langmuir*, 2002, **18**, 9696–9704.
165 R. Cruz-Silva, J. Romero-García, J. L. Angulo-Sánchez, A. Ledezma-Pérez, E. Arias-Marín, I. Moggio and E. Flores-Loyola, *Eur. Polym. J.*, 2005, **41**, 1129–1135.

Open Access Article. Published on 12 February 2026. Downloaded on 3/23/2026 6:55:17 AM.
This article is licensed under a Creative Commons Attribution 3.0 Unported Licence.

166 W. Liu, A. L. Cholli, R. Nagarajan, J. Kumar, S. Tripathy, F. F. Bruno and L. Samuelson, *J. Am. Chem. Soc.*, 1999, **121**, 11345–11355.
167 S. Yitzchaik, *J. Self-Assem. Mol. Electron.*, 2023, 1–16.
168 W. Liu, J. Kumar, S. Tripathy, K. J. Senecal and L. Samuelson, *J. Am. Chem. Soc.*, 1999, **121**, 71–78.
169 X. Wang, H. Schreuder-Gibson, M. Downey, S. Tripathy and L. Samuelson, *Synth. Met.*, 1999, **107**, 117–121.
170 J. Heinze, B. A. Frontana-Uribe and S. Ludwigs, *Chem. Rev.*, 2010, **110**, 4724–4771.
171 W. Schuhmann, C. Kranz, H. Wohlschläger and J. Strohmeier, *Biosens. Bioelectron.:X*, 1997, **12**, 1157–1167.
172 G. G. Wallace, M. Smyth and H. Zhao, *TrAC, Trends Anal. Chem.*, 1999, **18**, 245–251.
173 D. -H. Kim, S. M. Richardson-Burns, J. L. Hendricks, C. Sequera and D. C. Martin, *Adv. Funct. Mater.*, 2007, **17**, 79–86.
174 M. Hämmerle, W. Schuhmann and H.-L. Schmidt, *Sens. Actuators, B*, 1992, **6**, 106–112.
175 A. F. Diaz and J. A. Logan, *J. Electroanal. Chem. Interfacial Electrochem.*, 1980, **111**, 111–114.
176 R. Gupta, M. Singhal, S. K. Nataraj and D. N. Srivastava, *RSC Adv.*, 2016, **6**, 110416–110421.
177 E. M. Genies, A. A. Syed and C. Tsintavis, *Mol. Cryst. Liq. Cryst.*, 1985, **121**, 181–186.
178 E. M. Genies and C. Tsintavis, *J. Electroanal. Chem. Interfacial Electrochem.*, 1985, **195**, 109–128.
179 S. Patra, K. Barai and N. Munichandraiah, *Synth. Met.*, 2008, **158**, 430–435.
180 S. K. Mondal, K. R. Prasad and N. Munichandraiah, *Synth. Met.*, 2005, **148**, 275–286.
181 R. Balint, N. J. Cassidy and S. H. Cartmell, *Acta Biomater.*, 2014, **10**, 2341–2353.
182 M. A. Barakat, R. Kumar, T. Almeelbi, B. A. Al-Mur and J. O. Eniola, *J. Cleaner Prod.*, 2022, **330**, 129942.
183 Y. Bu and Z. Chen, *ACS Appl. Mater. Interfaces*, 2014, **6**, 17589–17598.
184 A. Lin, M. Ren, X. Tan, J. Ma, Y. Zhang, T. Yang, Y. Pei and J. Cui, *J. Cleaner Prod.*, 2022, **345**, 131058.
185 W. Shi, X. Liu, T. Deng, S. Huang, M. Ding, X. Miao, C. Zhu, Y. Zhu, W. Liu, F. Wu, C. Gao, S. Yang, H. Y. Yang, J. Shen and X. Cao, *Adv. Mater.*, 2020, **32**, 1907404.
186 L. Brožová, P. Holler, J. Kovářová, J. Stejskal and M. Trchová, *Polym. Degrad. Stab.*, 2008, **93**, 592–600.
187 T. Sen, S. Mishra and N. G. Shimpi, *RSC Adv.*, 2016, **6**, 42196–42222.
188 A. M. A. Henaish, B. I. Salem, T. M. Meaz, Y. A. Alibwaini, A.-W. Ajlouni, O. M. Hemeda and E. A. Arrasheed, *Opt. Mater.*, 2021, **119**, 111397.
189 H. Ali and E. S. Mansor, *Colloid Interface Sci. Commun.*, 2020, **39**, 100330.
190 M. Riaz, T. Munawar, F. Mukhtar, M. S. Nadeem, S. Manzoor, M. N. Ashiq and F. Iqbal, *J. Mater. Sci.: Mater. Electron.*, 2022, **33**, 24462–24476.
191 G. Ćirić-Marjanović, *Synth. Met.*, 2013, **170**, 31–56.
192 A. Arora, V. Jaswal, K. Singh and R. Singh, *Orient. J. Chem.*, 2016, **32**, 2035–2042.
193 M. S. S. Danish, L. L. Estrella, I. M. A. Alemaida, A. Lisin, N. Moiseev, M. Ahmadi, M. Nazari, M. Wali, H. Zaheb and T. Senjyu, *Metals*, 2021, **11**, 80.
194 R. Gusain, K. Gupta, P. Joshi and O. P. Khatri, *Adv. Colloid Interface Sci.*, 2019, **272**, 102009.
195 V. Van Tran, T. T. V. Nu, H.-R. Jung and M. Chang, *Polymers*, 2021, **13**, 3031.
196 A. Varghese, K. R. P. Sunajadevi and D. Pinheiro, *Energy Adv.*, 2025, **4**, 743–762.
197 V. K. Yemmireddy and Y. Hung, *Compr. Rev. Food Sci. Food Saf.*, 2017, **16**, 617–631.
198 C. Li, S. He, H. Mo, X. Xu, P. Yang and M. Liu, *Environ. Sci.:Water Res. Technol.*, 2025, **11**, 1369–1385.
199 S. K. Sahu, A. Palai and D. Sahu, *Sustainable Chem. Environ.*, 2024, **8**, 100162.
200 A. B. Djurišić, Y. H. Leung and A. M. Ching Ng, *Mater. Horiz.*, 2014, **1**, 400.
201 E. Pelizzetti and C. Minero, *Comments Inorg. Chem.*, 1994, **15**, 297–337.
202 S. H. S. Chan, T. Yeong Wu, J. C. Juan and C. Y. Teh, *J. Chem. Technol. Biotechnol.*, 2011, **86**, 1130–1158.
203 M. Batzill, *Energy Environ. Sci.*, 2011, **4**, 3275.
204 Z. Jiang, W. Wan, H. Li, S. Yuan, H. Zhao and P. K. Wong, *Adv. Mater.*, 2018, **30**, 1706108.
205 C. Y. Toe, J. Scott, R. Amal and Y. H. Ng, *J. Photochem. Photobiol., C*, 2019, **40**, 191–211.
206 P. Raizada, V. Soni, A. Kumar, P. Singh, A. A. Parwaz Khan, A. M. Asiri, V. K. Thakur and V.-H. Nguyen, *J. Materiomics*, 2021, **7**, 388–418.
207 F. T. Geldasa, M. A. Kebede, M. W. Shura and F. G. Hone, *RSC Adv.*, 2023, **13**, 18404–18442.
208 L. Zhang, P. Liu and Z. Su, *Polym. Degrad. Stab.*, 2006, **91**, 2213–2219.
209 S. Ameen, M. S. Akhtar, Y. S. Kim, O.-B. Yang and H.-S. Shin, *Colloid Polym. Sci.*, 2011, **289**, 415–421.
210 R. M. Mohamed and E. S. Aazam, *Appl. Catal., A*, 2014, **480**, 100–107.
211 S. Sarmah and A. Kumar, *Indian J. Phys.*, 2011, **85**, 713–726.
212 F. Wang, S. Min, Y. Han and L. Feng, *Superlattices Microstruct.*, 2010, **48**, 170–180.
213 X. Li, D. Wang, G. Cheng, Q. Luo, J. An and Y. Wang, *Appl. Catal., B*, 2008, **81**, 267–273.
214 A. Yadav, H. Kumar, R. Sharma and R. Kumari, *Colloid Interface Sci. Commun.*, 2021, **40**, 100339.
215 F. H. de O. Alves, O. A. Araújo, A. C. de Oliveira and V. K. Garg, *Surf. Interfaces*, 2021, **23**, 100954.
216 M. Lv, L. Yang, X. Wang, X. Cheng, Y. Song, Y. Yin, H. Liu, Y. Han, K. Cao, W. Ma, G. Qi and S. Li, *RSC Adv.*, 2019, **9**, 40694–40707.
217 Z. Cui, S. Tian, X. Liu, Q. Wang, S. Zeng and J. Si, *Colloids Surf., A*, 2023, **664**, 131111.
218 H. Zhang, Z. Wang, J. Zhang and K. Dai, *Chin. J. Catal.*, 2023, **49**, 42–67.
219 M. Dai, Z. He, P. Zhang, X. Li and S. Wang, *J. Mater. Sci. Technol.*, 2022, **122**, 231–242.

 © 2026 The Author(s). Published by the Royal Society of Chemistry

Open Access Article. Published on 12 February 2026. Downloaded on 3/23/2026 6:55:17 AM.
This article is licensed under a Creative Commons Attribution 3.0 Unported Licence.

220 M. Kumar, H. Singh Dosanjh, Sonika, J. Singh, K. Monir and H. Singh, *Environ. Sci.:Water Res. Technol.*, 2020, **6**, 491–514.
221 Z. Zhang, J. Sun, S. Mo, J. Kim, D. Guo, J. Ju, Q. Yu and M. Liu, *Chem. Eng. J.*, 2022, **431**, 134287.
222 Z. Yang, Z. Wu, W. Hua, Y. Xiao, G. Wang, Y. Liu, C. Wu, Y. Li, B. Zhong, W. Xiang, Y. Zhong and X. Guo, *Adv. Sci.*, 2020, **7**, 1903279.
223 J. Chen, M. Gu, S. Liu, T. Sheng and X. Zhang, *ACS Appl. Mater. Interfaces*, 2021, **13**, 16210–16217.
224 C. Lai, M. Zhang, B. Li, D. Huang, G. Zeng, L. Qin, X. Liu, H. Yi, M. Cheng, L. Li, Z. Chen and L. Chen, *Chem. Eng. J.*, 2019, **358**, 891–902.
225 Z. Cai, Y. Zhou, S. Ma, S. Li, H. Yang, S. Zhao, X. Zhong and W. Wu, *J. Photochem. Photobiol., A*, 2017, **348**, 168–178.
226 X.-S. Hu, Y. Shen, Y.-T. Zhang, H.-F. Zhang, L.-H. Xu and Y.-J. Xing, *J. Alloys Compd.*, 2017, **695**, 1778–1785.
227 J. Feng, J. Liu, X. Cheng, J. Liu, M. Xu and J. Zhang, *Adv. Sci.*, 2018, **5**, 1700376.
228 D. Ma, J.-W. Shi, Y. Zou, Z. Fan, X. Ji and C. Niu, *ACS Appl. Mater. Interfaces*, 2017, **9**, 25377–25386.
229 S. Liu, N. Zhang, Z.-R. Tang and Y.-J. Xu, *ACS Appl. Mater. Interfaces*, 2012, **4**, 6378–6385.
230 Y. Su, X. Xu, R. Li, X. Luo, H. Yao, S. Fang, K. Peter Homewood, Z. Huang, Y. Gao and X. Chen, *Chem. Eng. J.*, 2022, **429**, 132241.
231 S. Wang, B. Zhu, M. Liu, L. Zhang, J. Yu and M. Zhou, *Appl. Catal., B*, 2019, **243**, 19–26.
232 T. Di, B. Zhu, J. Zhang, B. Cheng and J. Yu, *Appl. Surf. Sci.*, 2016, **389**, 775–782.
233 Z. Jiang, J. Liu, M. Gao, X. Fan, L. Zhang and J. Zhang, *Adv. Mater.*, 2017, **29**, 1002.
234 Q. Li, X. Li, S. Wageh, A. A. Al-Ghamdi and J. Yu, *Adv. Energy Mater.*, 2015, **5**, 1500010.
235 A. Vázquez, D. B. Hernández-Uresti and S. Obregón, *Appl. Surf. Sci.*, 2016, **386**, 412–417.
236 D. You, B. Pan, F. Jiang, Y. Zhou and W. Su, *Appl. Surf. Sci.*, 2016, **363**, 154–160.
237 T. Feng, Y. Cao, R. Gao, G. Su, H. Li, B. Dong and L. Cao, *Int. J. Hydrogen Energy*, 2022, **47**, 9934–9945.
238 Z. Liang, Y. Xue, X. Wang, X. Zhang and J. Tian, *Mater. Today Nano*, 2022, **18**, 100204.
239 Y. Qin, K. Xiao, S. Sun, Y. Wang and C. Kang, *Appl. Surf. Sci.*, 2023, **616**, 156431.
240 L. Huang, J. Bao, W. Quan, X. Li, T. Zhao, Y. Ning, W. Lu, K. Liu, F. Ren and H. Tian, *J. Alloys Compd.*, 2023, **934**, 167948.
241 B. Ren, W. Shen, L. Li, S. Wu and W. Wang, *Appl. Surf. Sci.*, 2018, **447**, 711–723.
242 J. Tan, M. Yu, Z. Cai, X. Lou, J. Wang and Z. Li, *J. Colloid Interface Sci.*, 2021, **588**, 547–556.
243 M. Murugalakshmi, G. Mamba and V. Muthuraj, *Appl. Surf. Sci.*, 2020, **527**, 146890.
244 S. Kumar, N. Yadav, P. Kumar and A. K. Ganguli, *Inorg. Chem.*, 2018, **57**, 15112–15122.
245 X. Wang, X. Wang, J. Huang, S. Li, A. Meng and Z. Li, *Nat. Commun.*, 2021, **12**, 4112.
246 J. Wang, Y. Shi, H. Sun, W. Shi and F. Guo, *J. Alloys Compd.*, 2023, **930**, 167450.
247 R. Gao, B. Cheng, J. Fan, J. Yu and W. Ho, *Chin. J. Catal.*, 2021, **42**, 15–24.
248 Z. Mamiyev and N. O. Balayeva, *Catalysts*, 2022, **12**, 1316.
249 Z. Zhao, X. Li, K. Dai, J. Zhang and G. Dawson, *J. Mater. Sci. Technol.*, 2022, **117**, 109–119.
250 X.-L. Yin, G.-Y. He, B. Sun, W.-J. Jiang, D.-J. Xue, A.-D. Xia, L.-J. Wan and J.-S. Hu, *Nano Energy*, 2016, **28**, 319–329.
251 Z. Cui, R. Yuan, H. Chen, B. Zhou, B. Zhu and C. Zhang, *J. Water Proc. Eng.*, 2024, **59**, 104900.
252 F. Khan, M. Zahid, H. N. Bhatti and Y. Jamil, *Int. J. Environ. Sci. Technol.*, 2023, **20**, 4811–4826.
253 C.-S. Hwang and N.-C. Wang, *Mater. Chem. Phys.*, 2004, **88**, 258–263.
254 N. Ikenaga, N. Chiyoda, H. Matsushima and T. Suzuki, *Fuel*, 2002, **81**, 1569–1576.
255 J. LOU and C. CHANG, *Sep. Purif. Technol.*, 2007, **57**, 513–518.
256 E. Casbeer, V. K. Sharma and X.-Z. Li, *Sep. Purif. Technol.*, 2012, **87**, 1–14.
257 R. Jasrotia, N. Jaswal, J. Prakash, C. C. Kit, J. Singh and A. Kandwal, *J. Magnesium Alloys*, 2024, **12**, 490–505.
258 T. P. Oliveira, G. N. Marques, M. A. Macedo Castro, R. C. Viana Costa, J. H. G. Rangel, S. F. Rodrigues, C. C. dos Santos and M. M. Oliveira, *J. Mater. Res. Technol.*, 2020, **9**, 15001–15015.
259 C. Ramankutty, S. Sugunan and B. Thomas, *J. Mol. Catal. A: Chem.*, 2002, **187**, 105–117.
260 P. Lahiri and S. K. Sengupta, *J. Chem. Soc., Faraday Trans.*, 1995, **91**, 3489–3494.
261 R. M. Persoons, E. De Grave, P. M. A. de Bakker and R. E. Vandenberghe, *Phys. Rev. B:Condens. Matter Mater. Phys.*, 1993, **47**, 5894–5905.
262 S. J. Salih and W. M. Mahmood, *Heliyon*, 2023, **9**, e16601.
263 N. M. Mahmoodi, *Desalination*, 2011, **279**, 332–337.
264 H. S. Jarusheh, A. Yusuf, F. Banat, M. A. Haija and G. Palmisano, *J. Environ. Chem. Eng.*, 2022, **10**, 108204.
265 A. Soufi, H. Hajjaoui, R. Elmoubarki, M. Abdennouri, S. Qourzal and N. Barka, *Appl. Surf. Sci. Adv.*, 2021, **6**, 100145.
266 T. Dippong, E. A. Levei and O. Cadar, *Nanomaterials*, 2021, **11**, 1560.
267 G. Fan, J. Tong and F. Li, *Ind. Eng. Chem. Res.*, 2012, **51**, 13639–13647.
268 R. Yu, J. Zhao, Z. Zhao and F. Cui, *J. Hazard. Mater.*, 2020, **390**, 121998.
269 B. Janani, A. Syed, L. Sruthi, P. R. Sivaranjani, A. M. Elgorban, A. H. Bahkali, N. S. S. Zaghloul, M. M. Badawy, A. Das and S. S. Khan, *Colloids Surf., A*, 2021, **628**, 127307.
270 V. S. S. Mosali, M. Qasim, B. Mullamuri, B. Chandu and D. Das, *J. Nanosci. Nanotechnol.*, 2017, **17**, 8918–8924.
271 J. Li, Q. Xiao, L. Li, J. Shen and D. Hu, *Appl. Surf. Sci.*, 2015, **331**, 108–114.
272 F. Rodríguez-reinoso, *Carbon*, 1998, **36**, 159–175.
273 R. Leary and A. Westwood, *Carbon*, 2011, **49**, 741–772.

Open Access Article. Published on 12 February 2026. Downloaded on 3/23/2026 6:55:17 AM.
This article is licensed under a Creative Commons Attribution 3.0 Unported Licence.

274 S. Trivedi, K. Lobo and H. S. S. Ramakrishna Matte, in *Fundamentals and Sensing Applications of 2D Materials*, Elsevier, 2019, pp. 25–90.
275 J. Wang, F. Ma and M. Sun, *RSC Adv.*, 2017, **7**, 16801–16822.
276 H. Lu, J. Wang, M. Stoller, T. Wang, Y. Bao and H. Hao, *Adv. Mater. Sci. Eng.*, 2016, **2016**, 1–10.
277 S. Rathinavel, K. Priyadharshini and D. Panda, *Mater. Sci. Eng., B*, 2021, **268**, 115095.
278 R. Hou, W. Zhu, Y. Yue, J. Feng, A. Ishag, B. Zhang and Y. Sun, *Environ. Sci.: Nano*, 2024, **11**, 2302–2323.
279 O. J. Ajala, J. O. Tijani, M. T. Bankole and A. S. Abdulkareem, *Environ. Nanotechnol., Monit. Manage.*, 2022, **18**, 100673.
280 F. Khurshid, M. Jeyavelan and S. Nagarajan, *Synth. Met.*, 2021, **278**, 116832.
281 A. Carmalin Sophia, T. Arfin and E. C. Lima, in *A New Generation Material Graphene: Applications in Water Technology*, Springer International Publishing, Cham, 2019, pp. 439–471.
282 A. Ali, M. Shoeb, B. Li and M. A. Khan, *Mater. Sci. Semicond. Process.*, 2022, **150**, 106974.
283 M. Adel, M. A. Ahmed, M. A. Elabiad and A. A. Mohamed, *Environ. Nanotechnol., Monit. Manage.*, 2022, **18**, 100719.
284 M. Karamipour, S. Fathi and M. Safari, *Int. J. Environ. Anal. Chem.*, 2023, **103**, 3853–3864.
285 R. Zhao, Y. Li, J. Ji, Q. Wang, G. Li, T. Wu and B. Zhang, *Colloids Surf., A*, 2021, **611**, 125866.
286 M. Nasiri, H. Ahmadzadeh and A. Amiri, *Talanta*, 2021, **227**, 122078.
287 D. Luo and X. Zhang, *Int. J. Hydrogen Energy*, 2018, **43**, 5668–5679.
288 D. Vilela, J. Parmar, Y. Zeng, Y. Zhao and S. Sánchez, *Nano Lett.*, 2016, **16**, 2860–2866.
289 S. Wang, X. Li, Y. Liu, C. Zhang, X. Tan, G. Zeng, B. Song and L. Jiang, *J. Hazard. Mater.*, 2018, **342**, 177–191.
290 H. Wu, S. Lin, C. Chen, W. Liang, X. Liu and H. Yang, *Mater. Res. Bull.*, 2016, **83**, 434–441.
291 M. Mitra, S. T. Ahamed, A. Ghosh, A. Mondal, K. Kargupta, S. Ganguly and D. Banerjee, *ACS Omega*, 2019, **4**, 1623–1635.
292 Y. Lin, S. Wu, C. Yang, M. Chen and X. Li, *Appl. Catal., B*, 2019, **245**, 71–86.
293 S. Steplin Paul Selvin, A. Ganesh Kumar, L. Sarala, R. Rajaram, A. Sathiyan, J. Princy Merlin and I. Sharmila Lydia, *ACS Sustain. Chem. Eng.*, 2018, **6**, 258–267.
294 M. R. Abukhadra, M. Shaban and M. A. Abd El Samad, *Ecotoxicol. Environ. Saf.*, 2018, **162**, 261–271.
295 Y. Qing, Y. Li, L. Cao, Y. Yang, L. Han, P. Dansawad, H. Gao and W. Li, *Sep. Purif. Technol.*, 2023, **314**, 123545.
296 E. Girija Shankar, M. Aishwarya, A. Khan, A. B. V. K. Kumar and J. S. Yu, *Ceram. Int.*, 2021, **47**, 23770–23780.
297 K. Shoueir, A. R. Wassel, M. K. Ahmed and M. E. El-Naggar, *J. Photochem. Photobiol., A*, 2020, **400**, 112703.
298 Z. Liu, Y. E. Miao, M. Liu, Q. Ding, W. W. Tjiu, X. Cui and T. Liu, *J. Colloid Interface Sci.*, 2014, **424**, 49–55.
299 X. Wang, J. Zhang, K. Zhang, W. Zou and S. Chen, *RSC Adv.*, 2016, **6**, 44851–44858.
300 X. Zhang, J. Wu, G. Meng, X. Guo, C. Liu and Z. Liu, *Appl. Surf. Sci.*, 2016, **366**, 486–493.
301 P. Ahuja, S. K. Ujjain, I. Arora and M. Samim, *ACS Omega*, 2018, **3**, 7846–7855.
302 C. H. Hung, C. Yuan and H. W. Li, *J. Hazard. Mater.*, 2017, **322**, 243–253.
303 Q. Zhou, D. Zhao, Y. Sun, X. Sheng, J. Zhao, J. Guo and B. Zhou, *Chemosphere*, 2020, **252**, 126468.
304 K. Maeda, *J. Photochem. Photobiol., C*, 2011, **12**, 237–268.
305 J. Schneider, M. Matsuoka, M. Takeuchi, J. Zhang, Y. Horiuchi, M. Anpo and D. W. Bahnemann, *Chem. Rev.*, 2014, **114**, 9919–9986.
306 H. Marusawa, K. Ichikawa, N. Narita, H. Murakami, K. Ito and T. Tezuka, *Bioorg. Med. Chem.*, 2002, **10**, 2283–2290.
307 Z. Tan, S. Zhang, S.-F. Jiang, S. Chen and H. Jiang, *ACS ES&T Water*, 2024, **4**, 3016–3026.
308 S. Palliyalil, R. K. V. Chola, S. Vigneshwaran, N. C. Poovathumkuzhi, B. M. Chelaveettil and S. Meenakshi, *Environ. Technol. Innovation*, 2022, **28**, 102586.
309 Y. Zhao, X. Linghu, Y. Shu, J. Zhang, Z. Chen, Y. Wu, D. Shan and B. Wang, *J. Environ. Chem. Eng.*, 2022, **10**, 108077.
310 S. K K, A. Singh, S. K. Srivastava, A. Bhattacharya, A. Bhatnagar and A. K. Gupta, *Dalton Trans.*, 2025, **54**, 2403–2420.
311 M. Mitra, A. Ghosh, A. Mondal, K. Kargupta, S. Ganguly and D. Banerjee, *Appl. Surf. Sci.*, 2017, **402**, 418–428.
312 S.-W. Lv, J.-M. Liu, F.-E. Yang, C.-Y. Li and S. Wang, *Chem. Eng. J.*, 2021, **409**, 128269.
313 A. Balapure, J. Ray Dutta and R. Ganesan, *RSC Appl. Interfaces*, 2024, **1**, 43–69.
314 O. S. Ekande and M. Kumar, *J. Environ. Chem. Eng.*, 2021, **9**, 105725.
315 J. Fu, Q. Xu, J. Low, C. Jiang and J. Yu, *Appl. Catal., B*, 2019, **243**, 556–565.
316 K. K. Das, L. Paramanik and K. Parida, *Int. J. Hydrogen Energy*, 2021, **46**, 24484–24500.
317 X. Yu, Y. Tian, Y. Wei, K. Wang, Z. Liu, F. Yang, L. Chen and J. Zhang, *J. Alloys Compd.*, 2024, **1005**, 175998.
318 R. Kaur, S. D. Lawaniya, S. Kumar, N. Saini and K. Awasthi, *Appl. Phys. A:Mater. Sci. Process.*, 2023, **129**, 765.
319 Q. Li, Y. Xia, K. Wei, X. Ding, S. Dong, X. Jiao and D. Chen, *New J. Chem.*, 2019, **43**, 6753–6764.
320 S. Nayak, G. Swain and K. Parida, *ACS Appl. Mater. Interfaces*, 2019, **11**, 20923–20942.
321 V. K. Parida, S. K. Srivastava, S. Chowdhury and A. K. Gupta, *Chem. Eng. J.*, 2023, **472**, 144969.
322 R. Mishra, S. Bera, R. Chatterjee, S. Banerjee, S. Bhattacharya, A. Biswas, S. Mallick and S. Roy, *Appl. Surf. Sci. Adv.*, 2022, **9**, 100241.
323 Y. Xiao, Y. Jiang, E. Zhou, W. Zhang, Y. Liu, J. Zhang, X. Wu, Q. Qi and Z. Liu, *J. Mater. Sci. Technol.*, 2023, **153**, 205–218.
324 N. A. Chopan and H.-T.-N. Chishti, *New J. Chem.*, 2023, **47**, 15487–15505.
325 X. Yu, Y. Lin, H. Liu, C. Yang, Y. Peng, C. Du, S. Wu, X. Li and Y. Zhong, *J. Colloid Interface Sci.*, 2020, **561**, 379–395.

 © 2026 The Author(s). Published by the Royal Society of Chemistry

Open Access Article. Published on 12 February 2026. Downloaded on 3/23/2026 6:55:17 AM.
This article is licensed under a Creative Commons Attribution 3.0 Unported Licence.

326 A. M. Mohammed, S. S. Mohtar, F. Aziz, M. Aziz and A. Ul-Hamid, *J. Environ. Chem. Eng.*, 2021, **9**, 105065.
327 R. Nekooie, T. Shamspur and A. Mostafavi, *J. Photochem. Photobiol., A*, 2021, **407**, 113038.
328 Y. Chen, T. Wang, J. Pan, M. Wang, A. Chen and Y. Chen, *Bull. Mater. Sci.*, 2022, **45**, 45.
329 R. Tanwar, S. Kumar and U. K. Mandal, *J. Photochem. Photobiol., A*, 2017, **333**, 105–116.
330 T. Li, J.-D. Cui, L.-M. Gao, Y.-Z. Lin, R. Li, H. Xie, Y. Zhang and K. Li, *ACS Sustain. Chem. Eng.*, 2020, **8**, 13352–13361.
331 F. Mousli, A. Chaouchi, S. Hocine, A. Lamouri, M. Rei Vilar, A. Kadri and M. M. Chehimi, *Appl. Surf. Sci.*, 2019, **465**, 1078–1095.
332 X. P. Chen, J. K. Jiang, Q. H. Liang, N. Yang, H. Y. Ye, M. Cai, L. Shen, D. G. Yang and T. L. Ren, *Sci. Rep.*, 2015, **5**, 16907.
333 K. M. Molapo, P. M. Ndangili, R. F. Ajayi, G. Mbambisa, S. M. Mailu, N. Njomo, M. Masikini and P. B. I. Iwuoha, *Int. J. Electrochem. Sci.*, 2012, **7**, 11859–11875.
334 F. Amalina, A. S. A. Razak, S. Krishnan, A. W. Zularisam and M. Nasrullah, *Clean. Waste Syst.*, 2022, **3**, 100051.
335 M. Kadhom, N. Albayati, H. Alalwan and M. Al-Furaiji, *Sustainable Chem. Pharm.*, 2020, **16**, 100259.
336 M. Shaban, M. R. Abukhadra, A. A. P. Khan and B. M. Jibali, *J. Taiwan Inst. Chem. Eng.*, 2018, **82**, 102–116.
337 Z. Song, L. Chen, J. Hu and R. Richards, *Nanotechnology*, 2009, **20**, 275707.
338 T. Sauer, G. Cesconeto Neto, H. José and R. F. P. Moreira, *J. Photochem. Photobiol., A*, 2002, **149**, 147–154.
339 B. Zongo, F. Zongo, A. Toguyeni and J. I. Boussim, *J. For. Res.*, 2017, **28**, 1039–1048.
340 V. K. Gupta, D. Mohan and V. K. Saini, *J. Colloid Interface Sci.*, 2006, **298**, 79–86.
341 M. Shaban, A. M. Ashraf and M. R. Abukhadra, *Sci. Rep.*, 2018, **8**, 781.
342 O. A. Attallah, M. A. Al-Ghobashy, M. Nebsen and M. Y. Salem, *RSC Adv.*, 2016, **6**, 11461–11480.
343 M. S. Atas, S. Dursun, H. Akyildiz, M. Citir, C. T. Yavuz and M. S. Yavuz, *RSC Adv.*, 2017, **7**, 25969–25977.
344 E. Dhanda, A. Nain and S. Dahiya, *Water, Air, Soil Pollut.*, 2024, **235**, 1–16.
345 K. Pandiselvi, H. Fang, X. Huang, J. Wang, X. Xu and T. Li, *J. Hazard. Mater.*, 2016, **314**, 67–77.
346 Z. Lai, M. A. Ashwini, S. Sagadevan, D. Susanti and M. R. Johan, *J. Inorg. Organomet. Polym. Mater.*, 2025, DOI: 10.1007/s10904-025-04038-2.
347 V. Sharma, V. Maivizhikannan, V. N. Rao, S. Kumar, A. Kumar, A. Kumar, M. V. Shankar and V. Krishnan, *Ceram. Int.*, 2021, **47**, 10301–10313.
348 A. Bouziani, M. Yahya, C. L. Bianchi, E. Falletta and G. Celik, *Nanomaterials*, 2023, **13**, 713.
349 S. Shahabuddin, N. Muhamad Sarih, S. Mohamad and J. Joon Ching, *Polymers*, 2016, **8**, 27.
350 G. Sharma, M. Naushad, A. Kumar, S. Devi and M. R. Khan, *Iran. Polym. J.*, 2015, **24**, 1003–1013.
351 M. Faisal, M. Jalalah, F. A. Harraz, A. M. El-Toni, J. P. Labis and M. S. Al-Assiri, *Sep. Purif. Technol.*, 2021, **256**, 117847.
352 M. Asghar Jamal, S. Iqbal, S. Mahmood, S. Chohdry, A. Zidan, M. Tariq Qamar, M. Saeed, H. Asghar and K. M. Alotaibi, *Polyhedron*, 2024, **255**, 117137.
353 P. Hait, R. Mehta and S. Basu, *J. Cleaner Prod.*, 2023, **424**, 138851.
354 J. Ma, J. Dai, Y. Duan, J. Zhang, L. Qiang and J. Xue, *Renewable Energy*, 2020, **156**, 1008–1018.
355 F. Chen, W. Liang, X. Qin, L. Jiang, Y. Zhang, S. Fang and D. Luo, *ChemistrySelect*, 2021, **6**, 4166–4177.
356 A. Kumar, C. J. Raorane, A. Syed, A. H. Bahkali, A. M. Elgorban, V. Raj and S. C. Kim, *Environ. Res.*, 2023, **216**, 114741.
357 N. Turkten, Y. Karatas, S. Kurumoglu and Y. Yalcin Gurkan, *Phys. B*, 2025, **717**, 417802.
358 S. Zhao, Y. Tao, P. Maryum, Q. Wang, Y. Zhang, S. Li, H. Cheng, F. Min and Y. Tai, *Russ. J. Phys. Chem. A*, 2021, **95**, 1745–1755.
359 C. G. Daughton and T. A. Ternes, *Environ. Health Perspect.*, 1999, **107**, 907–938.
360 C. Zheng, J. Liu, Y. Cai, C. Jing, R. Jiang, X. Zheng and G. Lu, *Process Saf. Environ. Prot.*, 2022, **166**, 491–499.
361 R. Neha, S. Adithya, R. S. Jayaraman, K. P. Gopinath, P. M, P. L and J. Arun, *Chemosphere*, 2021, **272**, 129852.
362 S. Kar, K. Roy and J. Leszczynski, *Impact of Pharmaceuticals on the Environment: Risk Assessment Using QSAR Modeling Approach*, 2018, pp. 395–443.
363 B. Barik, S. J. Sahoo, B. Maji, J. Bag, M. Mishra and P. Dash, *Ind. Eng. Chem. Res.*, 2021, **60**, 15125–15140.
364 J. Wang, X. Yu, X. Fu, Y. Zhu and Y. Zhang, *Mater. Sci. Semicond. Process.*, 2021, **121**, 105329.
365 A. Kumar, M. Chandel, A. Sharma, M. Thakur, A. Kumar, D. Pathania and L. Singh, *J. Environ. Chem. Eng.*, 2021, **9**, 106159.
366 X. Tian, S. Liu, B. Zhang, S. Wang, S. Dong, Y. Liu, L. Feng and L. Zhang, *Environ. Res.*, 2023, **219**, 115035.
367 H. Ren, J. Li, Y. Niu, W. Zhang, Y. Lv, Y. Wang and C. Song, *Ind. Eng. Chem. Res.*, 2025, **64**, 8652–8664.
368 R. Kumar, M. A. Taleb, M. A. Barakat and B. Al-Mur, *Catalysts*, 2023, **13**, 175.
369 M. Anjum, M. Oves, R. Kumar and M. A. Barakat, *Int. Biodeterior. Biodegrad.*, 2017, **119**, 66–77.
370 A. Jilani, G. U. Rehman, M. O. Ansari, M. H. D. Othman, S. Z. Hussain, M. R. Dustgeer and R. Darwesh, *New J. Chem.*, 2020, **44**, 19570–19580.
371 S. Patnaik, K. K. Das, A. Mohanty and K. Parida, *Catal. Today*, 2018, **315**, 52–66.
372 M. Karamifar, S. Sabbaghi, M. S. Mohtaram, K. Rasouli, M. Mohsenzadeh, H. Kamyab, A. Derakhshandeh, L. Dolatshah, H. Moradi and S. Chelliapan, *Powder Technol.*, 2024, **432**, 119176.
373 W. Li, Y. Tian, C. Zhao, Q. Zhang and W. Geng, *Chem. Eng. J.*, 2016, **303**, 282–291.
374 J. Balasubramanian, S. K. Ponnaiah, P. Periakaruppan and D. Kamaraj, *Environ. Sci. Pollut. Res.*, 2020, **27**, 2328–2339.
375 S. Sharma, A. Sharma, N. S. Chauhan, M. Tahir, K. Kumari, A. Mittal and N. Kumar, *Inorg. Chem. Commun.*, 2022, **146**, 110093.

Open Access Article. Published on 12 February 2026. Downloaded on 3/23/2026 6:55:17 AM.
This article is licensed under a Creative Commons Attribution 3.0 Unported Licence.

376 A. Dolatkhah, P. R. Gupta, B. G. K. Steiger, M. Kazem-Rostami, M. Khani and L. D. Wilson, *Macromol. Chem. Phys.*, 2025, **226**, e00335.
377 N. Zare, R. K. Kojoori, S. Abdolmohammadi and S. Sadegh-Samiei, *J. Mol. Struct.*, 2022, **1250**, 131903.
378 S. Singh, P. Kaur, D. Aggarwal, V. Kumar, K. Tikoo, S. Bansal and S. Singhal, *J. Alloys Compd.*, 2022, **923**, 166255.
379 M. Schaffer and T. Licha, *Chemosphere*, 2014, **103**, 12–25.
380 X. Deng, Y. Chen, J. Wen, Y. Xu, J. Zhu and Z. Bian, *Sci. Bull.*, 2020, **65**, 105–112.
381 B. Amenu, A. M. Taddesse, T. Kebede, E. T. Mengesha and Z. Bezu, *Environ. Nanotechnol., Monit. Manage.*, 2024, **21**, 100926.
382 M. A. Alenizi, R. Kumar, M. Aslam, F. A. Alseroury and M. A. Barakat, *Sci. Rep.*, 2019, **9**, 12091.
383 J. Zhao, M. R. U. D. Biswas and W.-C. Oh, *Environ. Sci. Pollut. Res.*, 2019, **26**, 11888–11904.
384 B. Vishnu, S. Sriram and J. Jayabharathi, *New J. Chem.*, 2023, **47**, 5977–5990.
385 B. Barik, M. Mishra and P. Dash, *Environ. Sci.: Nano*, 2021, **8**, 2676–2692.
386 M. G. Galloni, C. Della Pina, V. Bortolotto, V. Nikonova, E. Falletta and C. L. Bianchi, *J. Mater. Sci.*, 2025, **60**, 5300–5325.

 © 2026 The Author(s). Published by the Royal Society of Chemistry